

SINGULAR BIFURCATIONS IN A SLOW-FAST MODIFIED LESLIE-GOWER MODEL WITH HOLLING TYPE II FUNCTIONAL RESPONSE, WEAK ALLEE EFFECT AND A GENERALIST PREDATOR

ROBERTO ALBARRAN GARCÍA, MARTHA ALVAREZ-RAMÍREZ,
AND HILDEBERTO JARDÓN-KOJAKHMETOV

ABSTRACT. We study a predator-prey system with a generalist Leslie-Gower predator, a functional Holling type II response, and a weak Allee effect on the prey. The prey's population often grows much faster than its predator, allowing us to introduce a small time scale parameter ε that relates the growth rates of both species, giving rise to a slow-fast system. Zhu and Liu (2022) show that, in the case of the weak Allee effect, Hopf singular bifurcation, slow-fast canard cycles, relaxation oscillations, etc., exist. Our main contribution lies in the rigorous analysis of a degenerate scenario organized by a (degenerate) transcritical bifurcation. The key tool employed is the blow-up method that desingularizes the degenerate singularity. In addition, we determine the criticality of the singular Hopf bifurcation using recent intrinsic techniques that do not require a local normal form. The theoretical analysis is complemented by a numerical bifurcation analysis, in which we numerically identify and analytically confirm the existence of a nearby Takens-Bogdanov point.

CONTENTS

| | |
|--|----|
| 1. Introduction | 2 |
| 2. Existence and types of positive equilibria | 4 |
| 3. Linear stability analysis of the positive equilibrium E_1 | 9 |
| 3.1. Linear stability analysis for the case $C < -AMQ$ | 9 |
| 3.2. Linear stability analysis for the <i>degenerate</i> case $C = -AMQ$ | 11 |
| 4. Analysis of the slow-fast model | 12 |
| 5. Intrinsic determination of the criticality of the singular Hopf bifurcation | 16 |
| 6. Desingularization of the point T_C , in the degenerate case $C = -AMQ$ | 20 |
| 6.1. Entry chart | 20 |
| 6.2. Central chart | 22 |
| 6.3. Exit Chart | 24 |
| 6.4. Bottom chart | 26 |
| 6.5. Blown-up dynamics at T_C , relaxation oscillations, and transitory canard | 27 |
| 7. Relaxation oscillations for $C < -AMQ$ | 30 |
| 8. Numerical analysis and validation | 34 |
| 9. Conclusions and Discussion | 34 |
| Appendix A. Expression for the trace of the Jacobian $\mathcal{J}(E_1)$ | 34 |
| Appendix B. Analytic determination of the Takens-Bogdanov bifurcation | 37 |

Key words and phrases. predator-prey model; slow-fast dynamical system; singular perturbations; blow-up; invariant manifolds.

1. INTRODUCTION

Mathematical ecology relies heavily on the analysis of predator-prey dynamics to forecast species interactions and the evolution, growth, and population distribution patterns of the biological species involved. The earliest predator-prey model based on sound mathematical principles was proposed by Lotka [27] and Volterra [37]. Following their findings, numerous attempts to improve them have been carried out since then. The Leslie-Gower model is one of the efforts to achieve this task, whose main characteristic is that the predator's growth equation is logistic, which implies that there is competition or self-interference between the predators, see [25]. Currently, the Leslie-Gower model has been studied from mathematical as well as biological viewpoints by many researchers, which is evident from the amount of published works, see for instance, [14], [20], [10], [31], [13] and references therein.

In 1931, the biologist W.C. Allee investigated population fluctuations and found out that a variety of biological phenomena affect species dynamics, such as mate-finding difficulties, social thermoregulation, genetic drift, avoidance of natural enemies, avoidance of predators, the defense of resources and poor nutrition due to low population densities. This phenomenon is now referred to as the *Allee effect*. Strong Allee effects result in critical population sizes, whereas weak Allee effects do not. This is due to the effect's link between population density or size to mean individual fitness. The readers who are interested in this topic are encouraged to refer to, e.g., [30], [3], [33].

The *functional response*, which refers to the amount of prey a predator consumes per unit of time, is a crucial component of mathematical models of predator-prey dynamics. The ability of the prey to flee an attack or the success of the predator's pursuit are two examples of the variables that it may affect. Numerous population studies have made the assumption that the functional response is of Holling type I, II, or III; see [17], [18]. The predator-prey model with a functional Holling type II response is the subject of this study. This type of response indicates that the predator spends more time hunting for prey at low prey densities and more time handling prey at high prey densities. A functional Holling type II response is expressed mathematically as:

$$h(x) = \frac{qx}{x+a},$$

where $x = x(t)$ represents the density of the prey population at time $t \geq 0$, q is the maximum per-capita consumption rate, and a is the average saturation rate, that is, the number of prey items at which the predation rate reaches half its maximum value.

As we will see in the main parts of this manuscript, we will eventually assume that the prey's evolution is considerably faster than that of the predator. In this regard, Geometric singular perturbation theory (GSPT) has been developed by Fenichel [11], Dumotier et al. [9, 8], Krupa and Szmolyan [22, 23], De Maesschalck et al. [4, 6], among many others, and it is an important theory that allows one to study systems with multiple time scales. GSPT is based on extensions of the classical normal hyperbolicity and transversality concepts. We refer the reader to [24] for a standard introductory treatment of the topic and to [5] for an overview of canard cycles for two-dimensional autonomous smooth slow-fast families of vector fields on manifolds, but especially a meticulous and unified treatment of canard cycles in dimension two. Nowadays, GSPT, together with normally hyperbolic theory, slow-fast normal form theory, and blow-up techniques, have been

used by several authors to study the dynamics of many versions of prey-predator models with multiple time scales. Without being exhaustive, we can mention the following works. Yao et al. [39] discussed the cyclicity of slow-fast cycles with two canard mechanisms in the modified Holling–Tanner model. Wen and Shi [38] showed the existence and uniqueness of canard cycles with cyclicity in a Leslie-Gower model are predator-prey with prey harvesting. Li et al. [26] proved the phenomenon of canard explosion and relaxation oscillations in a Lotka-Volterra system with Allee effect in the predator. Also, the singular slow-fast homoclinic orbit phenomenon has been investigated, e.g., Sahoo and Guruprasad [32] considered a predator-prey model with Beddington–DeAngelis functional response in which the prey reproduction is affected by the predation-induced fear and its carry-over effect. Using the GSPT and asymptotic expansion technique, they observed a wide range of rich and complex dynamics such as canard cycles (with or without head) near the singular Hopf-bifurcation threshold and relaxation oscillation cycles. In [34], Shen analyzed the existence and the nonexistence of canard limit cycles in a predator-prey system with a non-monotonic functional response. Yao and Huzak [40] studied the Leslie–Gower predator-prey model with Michaelis–Menten type prey harvesting. They focused on the cyclicity of diverse limit periodic sets, including a generic contact point, canard slow–fast cycles, transitory canards, slow–fast cycles with two canard mechanisms, singular slow–fast cycle, etc. In summary, extensive research has focused on exploring the dynamics of predator–prey models incorporating the Allee effect.

In particular, the model we consider is taken from Arancibia-Ibarra and Flores [1] who studied the Leslie-Gower predator-prey model with functional response Holling type II, Allee effect in the prey, and a generalist predator, which has the form [1]:

$$\begin{aligned}\frac{dx}{dt} &= rx \left(1 - \frac{x}{K}\right) (x - m) - \frac{qxy}{x + a}, \\ \frac{dy}{dt} &= sy \left(1 - \frac{y}{nx + c}\right),\end{aligned}\tag{1}$$

where x and y represent the size of the populations of prey and predator, respectively, at time t . The biological meanings of the parameters r , K , m , q , a , s , n , and c are displayed in Table 1.

| Parameter | Description |
|-----------|--|
| r | intrinsic prey growth rate |
| K | prey environmental carrying capacity |
| m | minimum viable population or Allee threshold |
| q | consuming maximum rate per capita of the predators |
| a | is the amount of prey to reach half of q |
| s | intrinsic predator growth rate |
| n | food quality and it indicates how the predators turn eaten prey into new predator births |
| c | environmental carrying capacity for the predator |

TABLE 1. Biological meanings of parameters in (1).

For its importance in the subsequent analysis, it is worth pointing out that the coordinate axes in system (1) are invariant for the dynamics. Due to the biological interpretation, we restrict our attention to system (1) in the first quadrant $\{(x, y) \in \mathbb{R}^2, x \geq 0, y \geq 0\}$. Arancibia-Ibarra and Flores [1] demonstrated that system (1) undergoes Hopf and Takens-Bogdanov bifurcations

when certain parameter relationships are found. However, this model can also be examined from a different perspective. For instance, Zhu and Liu [42] analyzed the same system, but assuming that the prey population increases much faster than that of the predators. This leads to a slow-fast system, and since the death rate for the predator is much less than for the prey, mathematically, it results in a singular perturbation problem. With the help of slow-fast normal form theory, geometric singular perturbation theory, and Fenichel's theory [11], they analyze some dynamical phenomena with strong ($m > 0$) and weak ($m < 0$) Allee effects, such as the existence of canard cycles related to a Hopf bifurcation, canard explosion and relaxation oscillations created by entry-exit function, and heteroclinic and homoclinic orbits.

This article revisits the slow-fast system (1) also considered by Zhu and Liu [42], focusing on a previously unaddressed degenerate case that displays intriguing dynamics characterized by the interaction of a Hopf and a degenerate transcritical singularities. This degenerate case occurs when the slow nullcline intersects the fast nullcline along the y -axis, as detailed in Section 2. In the vicinity of this case, we also uncover novel phenomena through numerical simulations that have not been previously reported. Moreover, we use modern techniques to evaluate the criticality of the organizing singularity. In contrast to the findings of Zhu and Liu [42], our analysis identifies the conditions under which degenerate relaxation oscillations persist in a scenario organized by a transcritical (degenerate) bifurcation.

The manuscript is organized as follows. In Section 2, we present the mathematical model for a modified Leslie–Gower predator–prey system incorporating an Allee effect on the prey and a Holling type II functional response. We also outline the parameter conditions required for the existence of equilibrium points, which are essential to our analysis. Section 3 contains the linear stability of these equilibrium points, highlighting its intrinsic dependence on the parameters. Assuming that the prey population grows significantly faster than the predator population, we formulate the slow-fast model in Section 4, where we explore the system using geometric singular perturbation theory, for the case of a unique positive equilibrium. Particularly, when the equilibrium point is a center, it is precisely located at the fold point. With this in mind, we then investigate the criticality of the slow-fast Hopf bifurcation using a formula from De Maesschalck et al. [4], which eliminates the need for normal form transformation. This approach is explained in detail in Section 5. In Section 6 we desingularize the degenerate transcritical singularity by means of the blow-up technique. This allows us to later show the existence of a transitory canard and of relaxation oscillations that pass through the aforementioned singularity. To the best of our knowledge, these degenerate scenarios have not been detailed before. For completeness, the existence of the relaxation oscillation in the generic setting is presented in Section 7. This article ends with the discussion section.

2. EXISTENCE AND TYPES OF POSITIVE EQUILIBRIA

Before we proceed into the details of the study, for the sake of simplicity, the following scalings are introduced:

$$\begin{aligned} x &= Ku, & y &= \frac{nK^2}{q}v, & d\tau &= \frac{rnK^3}{(nx+c)(u+a)}dt, & A &= \frac{a}{K} < 1, \\ C &= \frac{c}{Kn}, & S &= \frac{s}{rK}, & Q &= \frac{rK}{nq}, & M &= \frac{m}{K}, \end{aligned}$$

so that $(A, M, C, S, Q) \in (0, 1) \times (-1, 1) \times \mathbb{R}_+^3$. In this way, we have a system with only 5 free parameters. Substituting the new variables into system (1) and recycling t to denote the rescaled

time τ yields

$$\begin{aligned}\frac{du}{dt} &= u(u+C)\left((u+A)(1-u)(u-M)-v\right), \\ \frac{dv}{dt} &= Sv(u+A)(u+C-Qv).\end{aligned}\tag{2}$$

As the change of variables is only a scale transformation, systems (1) and (2) smoothly equivalent and then both systems have essentially the same phase portrait, except at the singularities $(nc+c)(u+a)=0$, which are not in the biologically meaningful domain. Our aim of this manuscript is to study the model (1) with weak Allee effect on the prey, that is (2) with $M < 0$.

The following result shows that the dynamics of the system, taking positive initial conditions, is contained in a region of the first quadrant. Moreover, the solutions are bounded, and they do not depend on the value of M . This fact is biologically important because of the achievability and finiteness of populations.

Proposition 1. *The set $\Gamma = \{(u, v) \in \mathbb{R}^2 : 0 \leq u \leq 1, v \geq 0\}$ is positively invariant under the flow of system (2). That is every orbit that enters Γ in finite time never leaves thereafter.*

Proof. It is straightforward to see that the u -axis ($v = 0$) and the v -axis ($u = 0$) are invariant sets because (2) is of Kolmogorov type [12]. If $u = 1$, we have that

$$\frac{du}{dt} = -(1+C)v < 0, \quad \text{for } v > 0$$

and whatever the sign of

$$\frac{dv}{dt} = Sv(1+A)(1+C-Qv),$$

the trajectories of the system get into the region Γ and cannot leave it once inside. \square

The next proposition establishes that all solutions initiating in Γ are eventually bounded.

Proposition 2. *All solutions of (2) with initial conditions in Γ are bounded and are contained in the set*

$$\tilde{\Gamma} = \left\{ (u, v) : 0 \leq u \leq 1, 0 \leq v \leq \frac{1+C}{Q} \right\},$$

as $t \rightarrow \infty$.

Proof. From the first equation in (2), we can see that for $(u, v) \in \Gamma$ and since $C > 0$,

$$\frac{du}{dt} \leq (1+A)(1+C)(1-u)(u-M),\tag{3}$$

Applying [2, lemma 2] to the differential inequality (3), one gets that:

$$u \leq \frac{Me^{-(1+A)(1+C)(1-M)t} - e^{c_1}}{e^{-(1+A)(1+C)(1-M)t} - e^{c_1}}.$$

Then, we obtain that $\limsup_{t \rightarrow \infty} u(t) \leq 1$.

Next, since $0 < u(t) < 1$ and $v > 0$, we have that

$$u+C-Qv < 1+C-Qv, \quad \text{for all } v \geq 0,$$

and also $Sv(u+C-Qv) < Sv(1+C-Qv)$. Moreover, $u+A < 1+A$ implies that $Sv(u+A)(u+C-Qv) < Sv(1+A)(1+C-Qv)$. Thus, from the second equation of (2), one has

$$\frac{dv}{dt} \leq Sv(1+A)(1+C-Qv).\tag{4}$$

Again, we apply [2, lemma 2] to (4), and after integrating the differential inequality and some manipulation, one obtains

$$v \leq \frac{1+C}{e^{-S(1+A)(1+C)t+(1+C)c_1} + Q}.$$

It follows that, $\limsup_{t \rightarrow \infty} v(t) \leq \frac{1+C}{Q}$. □

In the next stage, we will look for all feasible equilibrium points of (2). We note that the equilibrium points of (2) with $M > 0$ (strong Allee effect) and where one of the species goes extinct are $(M, 0)$, $(0, 0)$, $(0, C)$. On the other hand, if $M < 0$ (weak Allee effect), the equilibrium point $(M, 0)$ is found on the negative half-axis $u \leq 0$. Coexistence equilibrium points, in the presence of both populations, if any exist, correspond to the intersection of the nullclines in the first quadrant. These nullclines are given by

$$\ell(u) = \frac{u+C}{Q}, \quad \text{and} \quad h(u) = (u+A)(1-u)(u-M). \quad (5)$$

However, instead of looking for the intersection of these curves, we analyze the positive roots of the equivalent equation

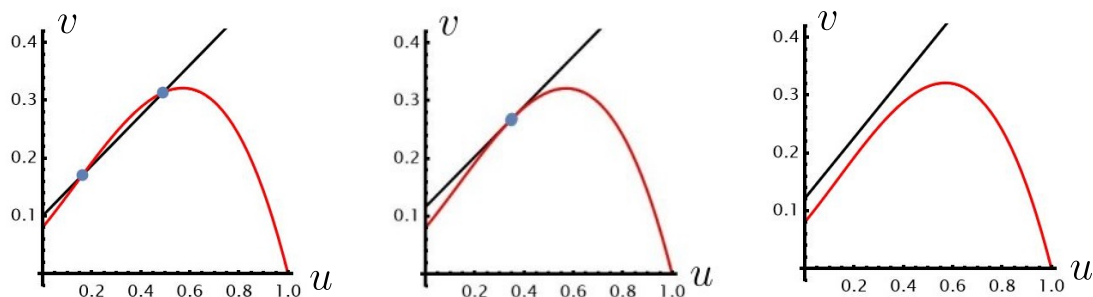
$$u^3 + (A-M-1)u^2 + \left(M-A-AM + \frac{1}{Q}\right)u + AM + \frac{C}{Q} = 0. \quad (6)$$

Remark 1. *The parameter $AM + \frac{C}{Q}$ is quite important. In the case $AM + \frac{C}{Q} = 0$, $u = 0$ is a solution of (6). In fact, as we will show below, when $AM + \frac{C}{Q} = 0$ the two nullclines $\ell(u)$ and $h(u)$ intersect at $T_C := (0, -AM)$ and define a degenerate scenario.*

Due to the difficulty of determining the exact solutions of equation (6), we use Descartes's rule of signs to give conditions under which (6) admits either three, two, one, or no positive roots. Therefore, the number of positive equilibria for system (2) is the same as that given in [1, Section 4] (although our rescaling of the variables is different from the one carried out in [1]). In short, we have the following.

Theorem 1. *For system (2), the following statements hold.*

1. *If $AM + \frac{C}{Q} > 0$ and $M < 0$, (see Figure 1) then*
 - (a) *If $A-M-1 < 0$ and $M-A-AM + \frac{1}{Q} \leq 0$ or $A-M-1 < 0$ and $M-A-AM + \frac{1}{Q} \geq 0$ or $A-M-1 \geq 0$ and $M-A-AM + \frac{1}{Q} < 0$, then the system (2) has up to two positive equilibrium points.*
 - (b) *If $A-M-1 > 0$ and $M-A-AM + \frac{1}{Q} \geq 0$ or $A-M-1 = 0$ and $M-A-AM + \frac{1}{Q} \geq 0$, then system (2) has no positive equilibrium points.*
2. *If $AM + \frac{C}{Q} = 0$ and $M < 0$, (see Figure 2) then*
 - (a) *If $A-M-1 < 0$ and $M-A-AM + \frac{1}{Q} > 0$, then system (2) has up to two positive equilibrium points.*
 - (b) *If $A-M-1 < 0$ and $M-A-AM + \frac{1}{Q} \leq 0$, or $A-M-1 \geq 0$ and $M-A-AM + \frac{1}{Q} < 0$, then system (2) has one positive equilibrium point.*
 - (c) *If $A-M-1 \geq 0$ and $M-A-AM + \frac{1}{Q} \geq 0$, then system (2) has no positive equilibrium points.*
3. *If $AM + \frac{C}{Q} < 0$ and $M < 0$, (see Figure 3) then*

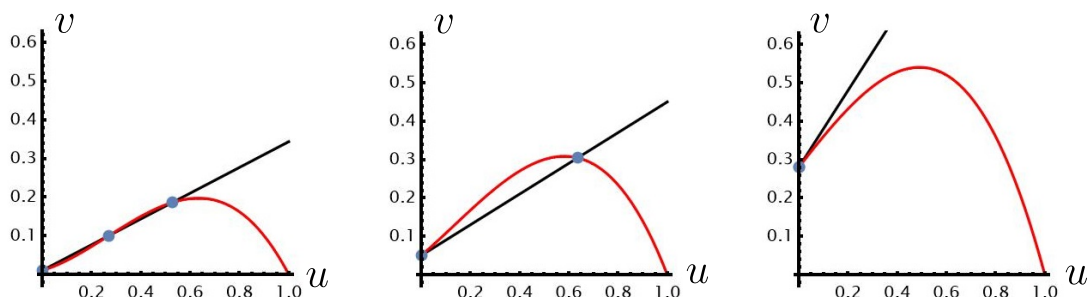


(a) The case 1a. in Theorem 1 with two equilibria.

(b) The case 1a. in Theorem 1 with one equilibrium.

(c) The case 1b. in Theorem 1 with no equilibria.

FIGURE 1. The intersection of the prey nullcline $h(u) = (u + A)(1 - u)(u - M)$ (red curve) and the predator nullcline $\ell(u) = (u + C)/Q$ (black line) for (2) with weak ($M < 0$) Allee effect. The intersection indicates two, one or zero positive equilibrium points of system.



(a) The case 2a. in Theorem 1 with two positive equilibria.

(b) The case 2b. in Theorem 1 with one positive equilibrium.

(c) The case 2c. in Theorem 1 without positive equilibria.

FIGURE 2. The intersection of the of the prey nullcline $h(u) = (u + A)(1 - u)(u - M)$ (red curve) and the predator nullcline $\ell(u) = (u + C)/Q$ (black line) for (2) with weak ($M < 0$) Allee effect. The intersection indicates two, one or zero positive equilibrium points of system.

- (a) If $A - M - 1 \leq 0$ and $M - A - AM + \frac{1}{Q} \leq 0$ or $A - M - 1 \geq 0$ and $M - A - AM + \frac{1}{Q} \geq 0$ or $A - M - 1 \geq 0$ and $M - A - AM + \frac{1}{Q} \leq 0$, then system (2) has one positive equilibrium point.
- (b) If $A - M - 1 < 0$ and $M - A - AM + \frac{1}{Q} > 0$, then system (2) has up to three positive equilibrium points.

Remark 2.

- Case 2 in Theorem 1 corresponds to a degenerate case where the two nullclines intersect along the v -axis, see Figure 2. It also serves as a separatrix of generic situations already

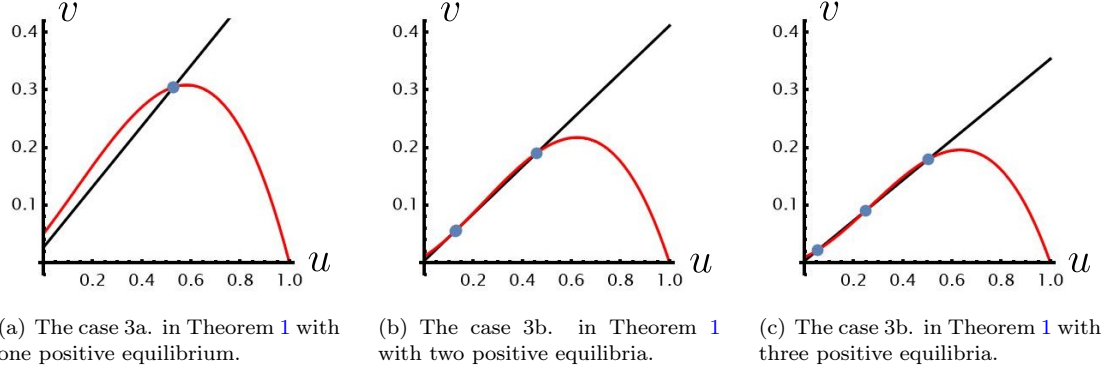


FIGURE 3. The intersection of the prey nullcline $h(u) = (u+A)(1-u)(u-M)$ (red curve) and the predator nullcline $\ell(u) = (u+C)/Q$ (black line) in the (2) model with weak ($M < 0$) Allee effect. The intersection indicates one or up to three positive equilibrium points of the system.

studied in the literature, see for instance [41]. Therefore, an important part of our paper is dedicated to such a case.

- Consider case 2 in Theorem 1 with A and M fixed. Let Q be sufficiently small such that there is exactly one positive equilibrium point (to be denoted as $E_1 = (U_1, V_1)$ in the rest of the paper). If $A - M - 1 < 0$ then, as one increases the value of Q , the coordinate U_1 decreases. Eventually, for $Q = \frac{1}{A-M+AM}$, a second equilibrium point (to be denoted $E_2 = (U_2, V_2)$ in the rest of the paper) appears (2(b) \rightarrow 2(a)). Further increasing Q makes E_1 collide with E_2 and disappear (2(a) \rightarrow 2(c)). On the other hand, if $A - M - 1 > 0$ then, as one increases the value of Q , the coordinate U_1 decreases. Eventually, E_1 collides with the origin before ceasing to exist (2(b) \rightarrow 2(c)).
- Consider case 3 in Theorem 1 with A and M fixed. Let Q be small enough that there is exactly one positive equilibrium point $E_1 = (U_1, V_1)$. If $A - M - 1 < 0$ then, as the value of Q is increased, the coordinate U_1 decreases. Moreover, for $Q = \frac{1}{A-M+AM}$ we have two cases:

- If $Q > \frac{3}{1+A+A^2-M+AM+M^2}$ a second equilibrium point $E_2 = (U_2, V_2)$ appears and eventually a third equilibrium point E_3 (3(a) \rightarrow 3(b)). When Q grows even more the points E_1 and E_2 collide and eventually disappear, while E_3 collides with the origin before ceasing to exist.
- If $Q < \frac{3}{1+A+A^2-M+AM+M^2}$, there is always only one equilibrium point.

On the other hand, if $A - M - 1 > 0$, we always have a unique equilibrium point. This because we are moving from one condition to another within those considered in item 3(a) of Theorem 1.

Remark 3. In the rest of the paper, we restrict ourselves to the case where there is only one equilibrium point for $C = -AMQ$ and $C < -AMQ$, but see section 8 for a further discussion. The case $C > -AMQ$ does not present oscillations, which are our main interest. Moreover, we notice

that $0 < Q < \frac{1}{A-M+AM}$ is necessary to have a unique positive equilibrium, which, in turn, implies that $A - M + AM > 0$.

3. LINEAR STABILITY ANALYSIS OF THE POSITIVE EQUILIBRIUM E_1

Since the u coordinate of the equilibrium point obtained from (6) has a very lengthy expression, namely

$$\mathcal{U}_1 = \frac{1}{6} \left(2^{2/3} \sqrt[3]{\alpha} + \frac{2 \sqrt[3]{2} (Q(A^2 + (A-1)M + A + M^2 + 1) - 3)}{Q \sqrt[3]{\alpha}} + 2(-A + M + 1) \right) \quad (7)$$

where

$$\begin{aligned} \alpha = & -2A^3 - 3A^2M - 3A^2 - \frac{9(-A + 3C + M + 1)}{Q} + 3AM^2 - 12AM + 3A + 2M^3 - 3M^2 \\ & - 3M + 2 + \left[\frac{1}{Q^3} \left(Q(2A^3Q + 3A^2(M+1)Q - 3A((M-4)MQ + Q + 3) + 27C \right. \right. \\ & \left. \left. - (M+1)((M-2)(2M-1)Q - 9) \right)^2 - 4(Q(A^2 + (A-1)M + A + M^2 + 1) - 3)^3 \right]^{1/2} \end{aligned}$$

we will simplify the presentation by using \mathcal{U}_1 as a parameter. The reader should keep in mind, however, that this is just a convenience, and \mathcal{U}_1 is entirely determined by the parameters of (2).

In order to discuss the stability of the positive equilibrium point, we need to compute the Jacobian matrix of system (2) with weak Allee effect ($M < 0$) at $E_1 = (\mathcal{U}_1, \mathcal{V}_1)$ with $0 < \mathcal{U}_1 < 1$ and $\mathcal{V}_1 = \frac{\mathcal{U}_1 + C}{Q}$. The resulting matrix is

$$\mathcal{J} = \begin{pmatrix} \mathcal{U}_1(\mathcal{U}_1 + C) \left(A - M + AM + 2(M + 1 - A)\mathcal{U}_1 - 3\mathcal{U}_1^2 \right) & -\mathcal{U}_1(\mathcal{U}_1 + C) \\ \frac{S(\mathcal{U}_1 + A)(\mathcal{U}_1 + C)}{Q} & -S(\mathcal{U}_1 + A)(\mathcal{U}_1 + C) \end{pmatrix}. \quad (8)$$

Thus, the trace and the determinant of \mathcal{J} are given by

$$\text{tr}(\mathcal{J}) = (\mathcal{U}_1 + C) \left((A - M + AM)\mathcal{U}_1 + 2(M + 1 - A)\mathcal{U}_1^2 - 3\mathcal{U}_1^3 - S(\mathcal{U}_1 + A) \right), \quad (9)$$

and

$$\det(\mathcal{J}) = S\mathcal{U}_1(\mathcal{U}_1 + A)(\mathcal{U}_1 + C)^2 \left(\frac{1}{Q} - (A - M + AM)\mathcal{U}_1 + 2(M + 1 - A)\mathcal{U}_1^2 - 3\mathcal{U}_1^3 \right), \quad (10)$$

respectively. It is clear that the signs of the eigenvalues are determined by $\text{tr}(\mathcal{J})$ and $\det(\mathcal{J})$.

3.1. Linear stability analysis for the case $C < -AMQ$. In the following theorem, we determine the local stability properties of the unique positive equilibrium for the case $C < -AMQ$. The reader should be warned that unlike what happens in [1], in this work, and similar to [42], we will use Q as the bifurcation parameter rather than S since Q allows us to give conditions on the position and stability of the point, while S only gives us conditions on the stability.

Theorem 2. Let the system (2) be such that, we are in case 3(a) of Theorem 1¹. Then, the system (2) has only one positive interior equilibrium point $E_1 = (\mathcal{U}_1, \mathcal{V}_1)$, which is:

1. a stable node if $3\mathcal{U}_1^2 - 2(M + 1 - A)\mathcal{U}_1 - (AM + A - M - \frac{1}{Q}) > 0$ and

$$Q > \frac{3(\mathcal{U}_1 + C)}{(S + M(\mathcal{U}_1 - 2) - \mathcal{U}_1)\mathcal{U}_1 + A(S - (\mathcal{U}_1 - 2)\mathcal{U}_1 + M(2\mathcal{U}_1 - 3))};$$

2. an unstable node if $3\mathcal{U}_1^2 - 2(M + 1 - A)\mathcal{U}_1 - (AM + A - M - \frac{1}{Q}) > 0$ and

$$Q < \frac{3(\mathcal{U}_1 + C)}{(S + M(\mathcal{U}_1 - 2) - \mathcal{U}_1)\mathcal{U}_1 + A(S - (\mathcal{U}_1 - 2)\mathcal{U}_1 + M(2\mathcal{U}_1 - 3))};$$

3. a linear center if $3\mathcal{U}_1^2 - 2(M + 1 - A)\mathcal{U}_1 - (AM + A - M - \frac{1}{Q}) > 0$ and

$$Q = \frac{3(\mathcal{U}_1 + C)}{(S + M(\mathcal{U}_1 - 2) - \mathcal{U}_1)\mathcal{U}_1 + A(S - (\mathcal{U}_1 - 2)\mathcal{U}_1 + M(2\mathcal{U}_1 - 3))}.$$

Remark 4. Due to the importance of the critical value of the parameter Q corresponding to the linear center, we shall denote

$$Q_H := \frac{3(\mathcal{U}_1 + C)}{(S + M(\mathcal{U}_1 - 2) - \mathcal{U}_1)\mathcal{U}_1 + A(S - (\mathcal{U}_1 - 2)\mathcal{U}_1 + M(2\mathcal{U}_1 - 3))}, \quad (11)$$

which, as we will see below, corresponds to the parameter value for which a singular Hopf bifurcation occurs.

Proof. In order to determine the stability, we must calculate the eigenvalues of the Jacobian matrix (8). We first note that (9) and (10) may be written as

$$\text{tr}(\mathcal{J}) = (\mathcal{U}_1 + C) \left(\mathcal{U}_1 J_{11} - S(\mathcal{U}_1 + A) \right), \quad (12)$$

and

$$\det(\mathcal{J}) = S\mathcal{U}_1(\mathcal{U}_1 + A)(\mathcal{U}_1 + C)^2 \left(\frac{1}{Q} - J_{11} \right), \quad (13)$$

respectively, with $J_{11} = A - M + AM + 2(1 - A + M)\mathcal{U}_1 - 3\mathcal{U}_1^2$. Then, the signs of $\text{tr}(\mathcal{J})$ and $\det(\mathcal{J})$ depend on the signs of the factors $\mathcal{U}_1 J_{11} - S(\mathcal{U}_1 + A)$ and $\frac{1}{Q} - J_{11}$, respectively. Therefore, if $\frac{1}{Q} - J_{11} < 0$, then $\det(\mathcal{J}) < 0$ and thus the equilibrium point is a saddle point.

Next, if $\frac{1}{Q} - J_{11} > 0$, it follows that $\det(\mathcal{J}) > 0$. Then, the behavior of the equilibrium point depends on the trace. For convenience, we do some algebraic manipulations to arrive at the fact that the expression (9) reduces to

$$\begin{aligned} \text{tr}(\mathcal{J}) = (\mathcal{U}_1 + C) & \left[3 \left(AM + \frac{1}{Q} \right) \right. \\ & \left. + \mathcal{U}_1 \left((A - M - 1)\mathcal{U}_1 + 2 \left(\frac{1}{Q} - A + M - AM \right) + \frac{1}{Q} \right) - S(\mathcal{U}_1 + A) \right]. \end{aligned} \quad (14)$$

We refer to Appendix A for the derivation of (14). Furthermore, after some algebraic manipulation, one obtains that $\text{tr}(\mathcal{J}) = 0$ at the critical value for case 3(a), i.e. with $C < -AMQ$,

¹Where $M < 0$, $C < -AMQ$, $A - M - 1 < 0$ and $M - A - AM + \frac{1}{Q} < 0$ or $A - M - 1 > 0$ and $M - A - AM + \frac{1}{Q} > 0$ or $A - M - 1 > 0$ and $M - A - AM + \frac{1}{Q} < 0$.

namely

$$Q_H = \frac{3(\mathcal{U}_1 + C)}{(S + M(\mathcal{U}_1 - 2) - \mathcal{U}_1)\mathcal{U}_1 + A(S - (\mathcal{U}_1 - 2)\mathcal{U}_1 + M(2\mathcal{U}_1 - 3))}.$$

If we assume that $Q = Q_H$ with $\det(\mathcal{J}) > 0$, we conclude that the matrix \mathcal{J} has a pair of conjugate, purely imaginary eigenvalues, so that the equilibrium E_1 is a centre. Whenever $Q > Q_H$ the (complex) eigenvalues of \mathcal{J} have negative real parts negative, thus E_1 is topologically a stable node, while $Q < Q_H$ implies that \mathcal{J} has eigenvalues with positive real parts such that the equilibrium point is, topologically, an unstable node. Considering these different possibilities for the two eigenvalues, we obtain the results. \square

In summary, from the above analysis assuming that $\frac{1}{Q} - J_{11} > 0$, we can say that E_1 is stable for $Q > Q_H$, and it is unstable for $Q < Q_H$. In addition, the equilibrium point E_1 loses its stability through a supercritical Hopf bifurcation at the bifurcation value $Q = Q_H$, which we further describe in Section 5, so E_1 is surrounded by a stable limit cycle. For more information on this subject, the reader is referred to [15].

We would like to highlight that we are focusing exclusively on the case where $\frac{1}{Q} - J_{11} > 0$, as oscillations naturally occur in this scenario, whereas the case $\frac{1}{Q} - J_{11} < 0$ is more complex.

3.2. Linear stability analysis for the *degenerate* case $C = -AMQ$. The following result is similar to Theorem 2, but for the degenerate case $C = -AMQ$.

Theorem 3. *Let the system (2) be such that, we are in case 2(b) of Theorem 1². Then, the system (2) has only one positive interior equilibrium point. Therefore, the equilibrium point $(\mathcal{U}_1, \frac{\mathcal{U}_1 + C}{Q})$ is:*

1. a stable node if $3\mathcal{U}_1^2 - 2(M + 1 - A)\mathcal{U}_1 - (AM + A - M - \frac{1}{Q}) > 0$ and

$$Q > \frac{3\mathcal{U}_1}{AS + (2A - 2M + 2AM + S)\mathcal{U}_1 + (M - A - 1)\mathcal{U}_1^2};$$

2. an unstable node if $3\mathcal{U}_1^2 - 2(M + 1 - A)\mathcal{U}_1 - (AM + A - M - \frac{1}{Q}) > 0$ and

$$Q < \frac{3\mathcal{U}_1}{AS + (2A - 2M + 2AM + S)\mathcal{U}_1 + (M - A - 1)\mathcal{U}_1^2};$$

3. a linear center if $3\mathcal{U}_1^2 - 2(M + 1 - A)\mathcal{U}_1 - (AM + A - M - \frac{1}{Q}) > 0$ and

$$Q = Q_H = \frac{3\mathcal{U}_1}{AS + (2A - 2M + 2AM + S)\mathcal{U}_1 + (M - A - 1)\mathcal{U}_1^2}. \quad (15)$$

Proof. The proof follows from that of Theorem 2 by substituting $C = -AMQ$. \square

The results above show that, within the case of a unique positive equilibrium, the unique equilibrium E_1 undergoes a Hopf bifurcation as the parameter Q is varied. We want to describe how this bifurcation leads to complex dynamics in the model. For this, we will exploit a slow-fast structure provided by the parameter S . This is developed in the following section.

²Where $M < 0$, $C = -AMQ$, $A - M - 1 > 0$ and $M - A - AM + \frac{1}{Q} < 0$ or $A - M - 1 < 0$ and $M - A - AM + \frac{1}{Q} < 0$.

4. ANALYSIS OF THE SLOW-FAST MODEL

Species that belong to different trophic levels have distinct growth rates, which may differ by several orders of magnitude. In particular, there is empirical evidence of the interaction between species such as insects and birds [28], lynx and hares [35], etc., that show that the growth rate of the prey is often much faster than that of its predator. Based on these observations, several researchers have considered a mathematical prey-predator model accounting for the difference in time-scale. More specifically, one introduces a small time-scale parameter ε , $0 < \varepsilon \ll 1$ in the basic model. The parameter ε is interpreted as the ratio between the linear death rate of the predator and the linear growth rate of the prey [16], and the assumption $\varepsilon < 1$ implies that one generation of predator can encounter many different generations of prey.

In this section, we study the dynamics of (2) under the assumption that the prey population grows much faster than the predator's so that $s \ll r$. Since K , the carrying capacity for the prey population, usually has a value greater than 1, then $S = \frac{s}{rK}$ is a perturbation parameter that is small enough. Consequently, system (2) can be regarded as a slow-fast system [24] with a fast time scale t , where u is a fast variable, and v is a slow variable. The slow-fast model is given by the following system of equations:

$$\begin{aligned} \frac{du}{dt} &= f(u, v) = u(u + C)((u + A)(1 - u)(u - M) - v), \\ \frac{dv}{dt} &= \varepsilon g(u, v) = \varepsilon v(u + A)(u - Qv + C). \end{aligned} \tag{16}$$

where $\varepsilon > 0$ is a small parameter.

In the limiting case $\varepsilon \rightarrow 0$, the system (16) yields the *layer* (or *fast*) *problem*:

$$\begin{aligned} \frac{du}{dt} &= u(u + C)((u + A)(1 - u)(u - M) - Qv), \\ \frac{dv}{dt} &= 0, \end{aligned} \tag{17}$$

where the slow variable v can be treated as a parameter in the first equation. Next, by re-writing system (16) on the slow time scale $\tau = \varepsilon t$, we obtain

$$\begin{aligned} \varepsilon \frac{du}{d\tau} &= f(u, v) = u(u + C)((u + A)(1 - u)(u - M) - v), \\ \frac{dv}{d\tau} &= g(u, v) = v(u + A)(u - Qv + C). \end{aligned} \tag{18}$$

Taking the singular limit as $\varepsilon \rightarrow 0$ in system (18) leads to the *reduced* (or *slow*) *problem*:

$$\begin{aligned} 0 &= f(u, v) = u(u + C)((u + A)(1 - u)(u - M) - v), \\ \frac{dv}{d\tau} &= g(u, v) = v(u + A)(u - Qv + C), \end{aligned} \tag{19}$$

which is a differential-algebraic system.

The equilibria of the layer subsystem (18) define the critical manifold

$$\mathcal{M}_0 = \{(u, v) \in \mathbb{R}_+^2 \mid u(u + C)((u + A)(1 - u)(u - M) - v) = 0\},$$

composed of two submanifolds, namely

$$\begin{aligned} \mathcal{M}_0^0 &= \{(u, v) \in \mathbb{R}_+^2 \mid u = 0, v \geq 0\}, \\ \mathcal{M}_0^1 &= \{(u, v) \in \mathbb{R}_+^2 \mid v = (u + A)(1 - u)(u - M) = h(u), \text{ with } 0 < u < 1, v > 0\}, \end{aligned}$$

such that $\mathcal{M}_0 = \mathcal{M}_0^0 \cup \mathcal{M}_0^1$. Indeed, \mathcal{M}_0^0 is the positive v -axis and the \mathcal{M}_0^1 is cubic-shaped. Notice that \mathcal{M}_0 is the phase space of the reduced system (19).

Since $0 \leq u \leq 1$, we note that \mathcal{M}_0^1 has a unique zero at $u = 1$ and its intersection with the positive v -axis is the point $T_C = (0, v_C)$, with $v_C = -AM > 0$, since $M < 0$. We remark that the shape of \mathcal{M}_0 plays a key role in determining the behavior of system (16). Now, from the derivative

$$\frac{dh}{du} = -3u^2 + 2(1 - A + M)u + (A - M + AM), \quad (20)$$

it can be verified that the function $h(u)$ has a unique maximum point at $P := (u_p, v_p)$ in \mathcal{M}_0^1 , where

$$\begin{aligned} u_p &= \frac{1}{3}(1 - A + M + \beta), \\ v_p &= \frac{1}{27}(1 - A - 2M + \beta)(2 + A - M - \beta)(1 + 2A + M + \beta), \end{aligned} \quad (21)$$

with $\beta = \sqrt{A^2 + AM + A + M^2 - M + 1}$. The shape of the critical curve is illustrated in Figure 4.

Next, one can verify from (20), that

$$\frac{dh}{du} \begin{cases} > 0, & 0 < u < u_p, \\ < 0, & u_p < u < 1. \end{cases} \quad (22)$$

Therefore, we define the attracting and repelling branches of \mathcal{M}_0^1 as:

$$\begin{aligned} \mathcal{M}_0^{1,r} &= \{(u, v) \in \mathcal{M}_0^1 \mid 0 \leq u < u_p\}, \\ \mathcal{M}_0^{1,a} &= \{(u, v) \in \mathcal{M}_0^1 \mid u_p < u \leq 1\}, \end{aligned} \quad (23)$$

see again Figure 4.

Remark 5. Notice that, for the case of unique positive equilibrium, its stability has already been characterized in Theorems 2 and 3. In particular, the case when the equilibrium point is a center occurs when the equilibrium point is located exactly at the fold point P .

Regarding the flow in the critical curve \mathcal{M}_0^0 , taking into account that the line $u = 0$ is invariant according to the Proposition 1, it is possible to establish that

$$\left. \frac{dv}{d\tau} \right|_{u=0} = Av(c - Qv) \begin{cases} > 0, & \text{if } 0 < v < \frac{c}{Q}, \\ < 0, & \text{if } \frac{c}{Q} < v. \end{cases} \quad (24)$$

Next, we study the slow reduced dynamics on the critical manifold \mathcal{M}_0^1 . The slow dynamics along \mathcal{M}_0^1 is given by the following equation

$$\left. \frac{du}{d\tau} \right|_{\mathcal{M}_0^1} = \frac{g(u, h(u))}{h'(u)}, \quad (25)$$

where $g(u, v) = \frac{dv}{d\tau}$ and $h(u)$ are given in (5). So, it is possible to establish that

$$\left. \frac{du}{d\tau} \right|_{\mathcal{M}_0^1} = \frac{g(u, h(u))}{h'(u)} = \frac{h(u)(u + A)(u + C - Qh(u))}{h'(u)} \quad (26)$$

The sign of (25) depends on the sign of $g(u, h(u))$ and $h'(u)$. Notice that $h'(u) = 0$ at the fold point P . So, we proceed with the desingularization [36] by multiplying (26) by $h'(u)$ (we can also divide out $h(u)(u + A)$) to get the desingularized equation

$$\frac{du}{d\tau} = u + C - Qh(u). \quad (27)$$

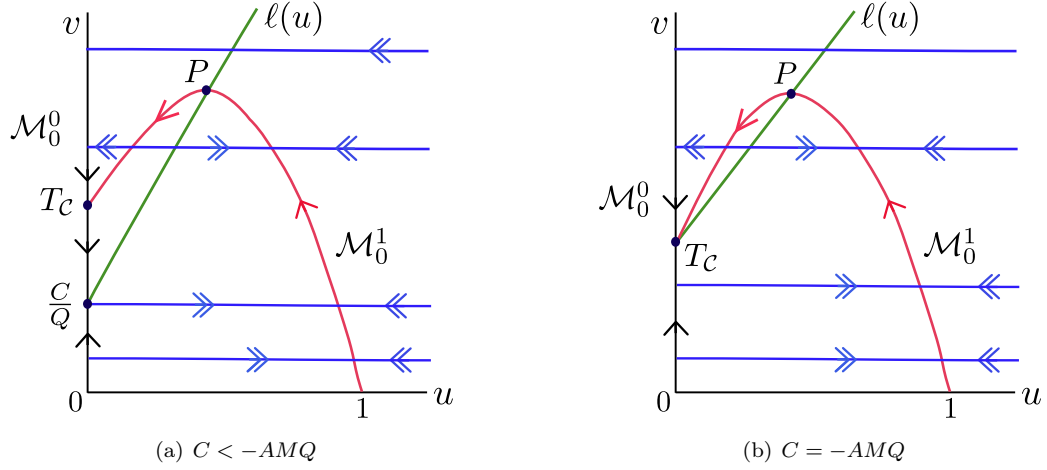


FIGURE 4. Dynamics of the slow-fast system (16) for (a) $C < -AMQ$ and (b) $C = -AMQ$, where \mathcal{M}_0^0 and \mathcal{M}_0^1 are the critical submanifolds. The fold point $P = (u_p, v_p)$ and $T_C = (0, -AM)$ are shown, as well as a schematic representation of the slow flow in the different components of the critical manifold. The green line $\ell(u)$ denotes the nullcline of variable the v . Hence, we are depicting the case in which an equilibrium of the slow flow coincides with the fold point, which may lead to canards, and corresponds to the parameter $Q = Q_H$. Indeed, in the figures, the magenta curve is a singular canard orbit.

Remark 6. We recall that the desingularized equation gives the flow in the correct direction for regions of the critical manifold where $h'(u) > 0$, and one must reverse the flow in regions where $h'(u) < 0$.

We further notice that an equivalent expression for \mathcal{U}_1 is $\mathcal{U}_1 = \{u + C - Qh(u) = 0\}$, provided we stay within the parameter's range leading to a unique equilibrium point. Next, let $u = \mathcal{U}_1$. The linearization of (27) at \mathcal{U}_1 is $1 - Qh'(\mathcal{U}_1)$. That is, if $h'(\mathcal{U}_1) > \frac{1}{Q}$, then \mathcal{U}_1 is stable, and if $h'(\mathcal{U}_1) < \frac{1}{Q}$, then \mathcal{U}_1 is unstable. Due to its biological meaning, we are interested in the case where the equilibrium point \mathcal{U}_1 is stable for $h'(u) < 0$ (i.e. on the attracting branch of the critical manifold). Given the desingularization process, we indeed verify that

- i) $g(u, h(u)) < 0$ when $u + C - Qh(u) < 0$, that is, when $0 < u < \mathcal{U}_1$,
- ii) $g(u, h(u)) > 0$ when $u + C - Qh(u) > 0$, that is, when $\mathcal{U}_1 < u < 1$,
- iii) $h'(u) > 0$ when $0 < \mathcal{U}_1 < u_p$,
- iv) $h'(u) < 0$ when $u_p < \mathcal{U}_1 < 1$.

Therefore, we have the following cases

- (1) If $h'(u) > 0$

$$\left. \frac{du}{d\tau} \right|_{\mathcal{M}_0^1} \begin{cases} < 0, & \text{if } 0 < u < \mathcal{U}_1, \\ > 0, & \text{if } \mathcal{U}_1 < u < 1. \end{cases}$$

(2) If $h'(u) < 0$

$$\left. \frac{du}{d\tau} \right|_{\mathcal{M}_0^1} \begin{cases} > 0, & \text{if } 0 < u < \mathcal{U}_1, \\ < 0, & \text{if } \mathcal{U}_1 < u < 1. \end{cases}$$

These cases correspond to the sketches in figure 5.

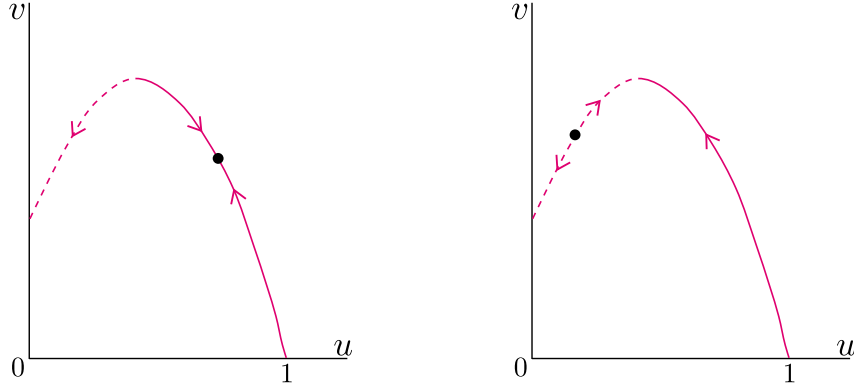


FIGURE 5. Slow flow when the equilibrium point E_1 is in either normally hyperbolic branch of \mathcal{M}_0^1 .

(3) When the equilibrium point E_1 coincides with the fold point P , that is $\mathcal{U}_1 = u_p$, then $g(u, h(u)) = 0$ and $h'(u) = 0$ for $Q = Q_H$. In this case, the right-hand side of (25) is an indeterminate form. Thus, we apply L'Hospital's rule obtaining

$$\left. \frac{du}{d\tau} \right|_{u=u_p} = \lim_{u \rightarrow u_p} \frac{g(u, h(u))}{h'(u)} = \lim_{u \rightarrow u_p} \frac{g_u(u, h(u))}{h''(u)} = \frac{h(u)(u+A)}{h''(u)} < 0, \quad (28)$$

which shows that, as sketched in Figure 4, the flow in \mathcal{M}_0^1 is directed towards the fold point P from the attracting side and away from it on the repelling side.

Now, we stress that Fenichel's theory [11] implies that the manifold \mathcal{M}_0^1 is normally hyperbolic except at the points P and T_C . Thus, any trajectory starting near the attracting (resp. repelling) submanifold $\mathcal{M}_0^{1,a}$ (resp. $\mathcal{M}_0^{1,r}$) cannot cross the fold point P (resp. T_C). On the other hand, the manifolds $\mathcal{M}_\varepsilon^{1,a}$ (resp. $\mathcal{M}_\varepsilon^{1,r}$) exist as a smooth perturbation of $\mathcal{M}_0^{1,a}$ (resp. $\mathcal{M}_0^{1,r}$). However, Fenichel's theory only guarantees the existence of such manifolds away from the fold point P and T_C . Our goal is to qualitatively describe the orbits of (2) in a small neighborhood of the singular points P and T_C and to describe later on the global dynamics organized by such singularities. We are going to use a suitable, but singular, coordinate change known as *blow-up* [24], which will induce a new system with only (semi-)hyperbolic equilibrium points and, therefore, can be analyzed with standard tools from dynamical systems theory.

We now turn our attention to the fold point $P = (u_p, v_p)$. Let us recall that a *generic* fold point is characterized by the following conditions

$$\frac{\partial f}{\partial u}(u_p, v_p) = 0, \quad \frac{\partial f}{\partial v}(u_p, v_p) \neq 0, \quad \frac{\partial^2 f}{\partial u^2}(u_p, v_p) \neq 0, \quad \text{and} \quad g(u_p, v_p) \neq 0,$$

while a non-generic one further satisfies $g(u_p, v_p) = 0$ [21]. The local dynamics along \mathcal{M}_0 near the fold point P can be distinguished between such two cases:

- A generic fold point P of the slow subsystem is singular and solutions reach P in finite forward or backward time. This case is known as jump point or regular contact point, which provides a condition for relaxation oscillations.
- A canard point is a fold point P with an additional degeneracy leading to a possibility of a canard solution. As a result, the system has a solution passing through P from the attracting to the repelling branch of the critical manifold M_0 .

The previous description is by now well-known, and we provide no further details but refer the reader to Figure 6 for a schematic of both cases, see also the textbooks [24] and [5].

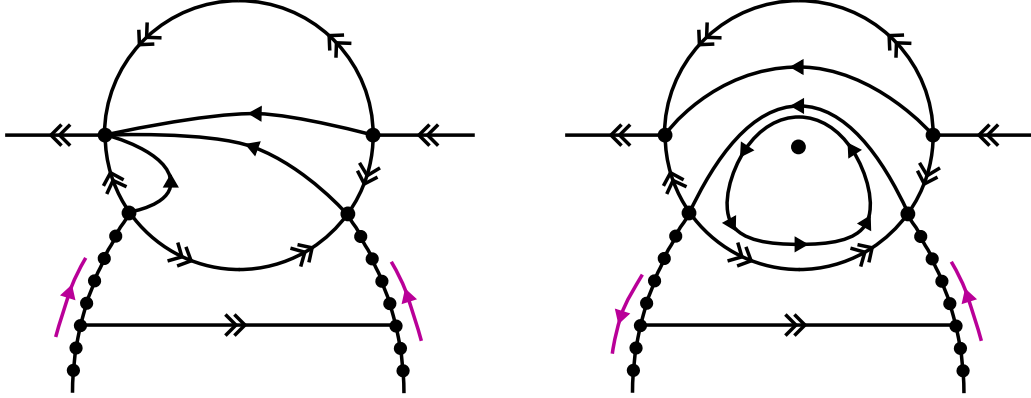


FIGURE 6. Left: schematic of the blow-up of a generic fold point. Right: schematic of the blow-up of a canard point. For these pictures we have used the local setup of the model under study. Hence, the right branch of the critical manifold is attracting, while the left branch is repelling. In the left picture, the slow flow (magenta) is directed toward the fold point on both branches of the critical manifold. On the right picture, the slow flow “passes through” the fold point, compare with Figure 4.

Usually, a canard point can alternatively be seen as a singular Hopf point. Whether the cycles that appear upon the bifurcation are stable or unstable depends on the criticality of the Hopf point. Until recently, determining the criticality requires putting the system into a normal form, which may sometimes be undesirable or unattainable. Recently, [4] proposes an intrinsic method to determine the criticality of a singular Hopf point; we shall apply such a method to our model in the following section and show that the canard point is indeed a (singular) supercritical Hopf point within a meaningful range of parameter values, which justifies the right-hand picture of Figure 6.

We emphasize that Zhu and Liu [42] already proved the occurrence of canard cycles and relaxation oscillations in the generic scenario $C \neq -AMQ$. Our main objective in the rest of the document will be to show the existence of the singular cycles shown in Figure 7 and to prove that such singular cycles perturb to nearby ones for $\varepsilon > 0$ sufficiently small.

5. INTRINSIC DETERMINATION OF THE CRITICALITY OF THE SINGULAR HOPF BIFURCATION

By using the inherent properties of the notion of a slow-fast Hopf point, De Maesschalck et al. [4] prove that the criticality of a slow-fast Hopf can be determined without the necessity of

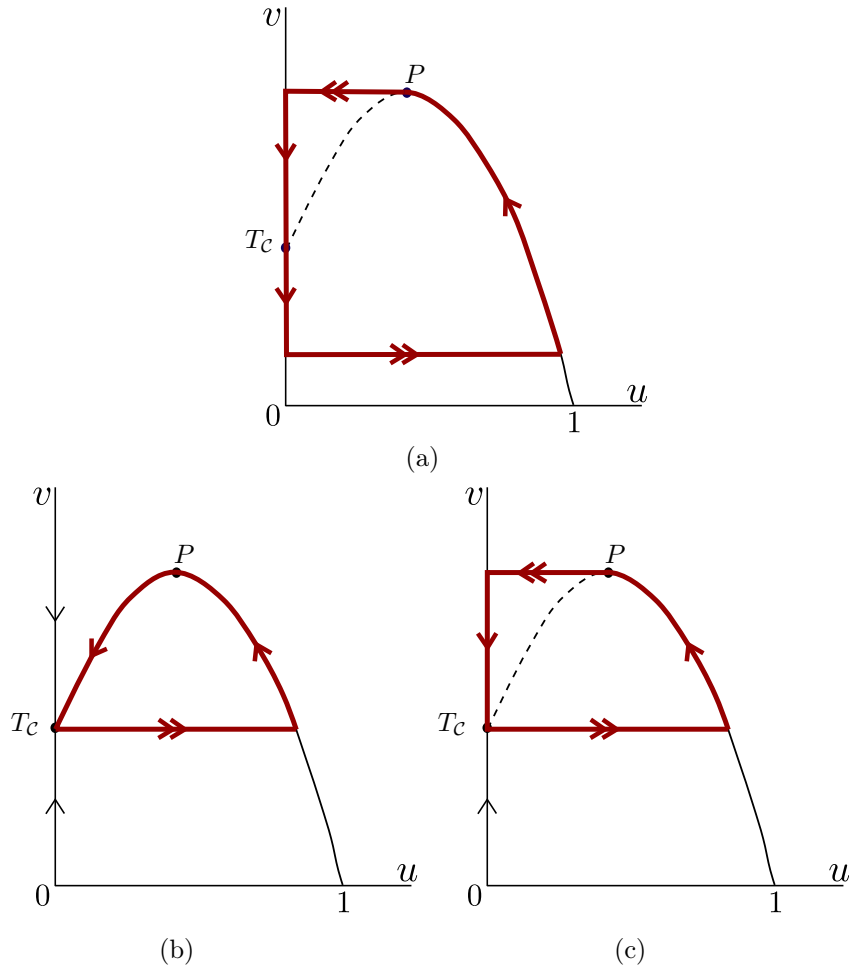


FIGURE 7. Singular cycles that we focus on. The solid red cycle in (a) represents a candidate orbit for a regular relaxation oscillation, which appear when $C < -AMQ$. Such a cycle has already been studied in [42], but here we include its analysis for completeness, see Section 7. The two on the bottom (b) and (c) are degenerate and, to the best of our knowledge, novel. At the singular level, they exist for $C = -AMQ$. As we show in Section 6, the one depicted in (b), called a transitory canard, is obtained by combining a maximal canard at P and a (degenerate) saddle-like transition at T_c . The one depicted in (c) combines a generic jump at P and the same degenerate saddle-like transition at T_c .

having or changing to a normal form. The authors present a single intrinsic formula for an intrinsic determination that verifies if any singular contact point of Hopf type exists and its criticality. Such an intrinsic formulation is beneficial because the critical curve does not require a parametrization.

We use such a technique in the following to show that system (16) may undergo a supercritical Hopf bifurcation as the parameter Q passes through Q_H .

Following [4], in this section, we deal with a slow-fast Hopf point in (16) at $P = (u_p, v_p)$ for $Q = Q_H$. Through the analysis of this section, we show that within a meaningful range of parameters, such a Hopf point is supercritical.

Considering the system (16), we define

$$\begin{aligned}\mathcal{F}(u, v) &= u(u + C)((u + A)(1 - u)(u - M) - v), \\ \mathcal{Q}(u, v) &= v(u + A)(u - Qv + C).\end{aligned}$$

The techniques of [4] apply to vector fields on 2-manifolds, however, it suffices for us to take the standard Euclidean metric, and associated area form. Using the formulas and the same notation as in [4], for $Z = \frac{\partial}{\partial u}$, we compute

$$\begin{aligned}Z\mathcal{F}(u, v) &= u(u + C)(A(1 + M - 2u) + (2 - 3u)u + M(2u - 1)) \\ &\quad + u((M - u)(u - 1)(A + u) - v) + (u + C)((M - u)(u - 1)(A + u) - v),\end{aligned}$$

$$\begin{aligned}ZZ\mathcal{F}(u, v) &= 2(-3Mu + 6u^2 + 6Mu^2 - 10u^3 + C(-M + 3u + 3Mu - 6u^2)) \\ &\quad + A(-M + C(1 + m - 3u) + 3u + 3Mu - 6u^2) - v),\end{aligned}$$

$$ZZZ\mathcal{F}(u, v) = 6(-M + C(1 + M - 4u) + A(1 - C + M - 4u) + 4u + 4Mu - 10u^2).$$

At this moment we point out that $P = (u_p, v_p)$ is a generic contact point, since one can check that, generically (for $Q \neq Q_H$)

$$\mathcal{F}(P) = 0, \quad Z\mathcal{F}(P) = 0, \quad ZZ\mathcal{F}(P) \neq 0.$$

We now compute

$$\det(\mathcal{Q}, Z) = \begin{vmatrix} 0 & 1 \\ \mathcal{Q}(u, v) & 0 \end{vmatrix} = -v(u + A)(u - Qv + C),$$

and

$$\begin{aligned}\det(\nabla\mathcal{F}, \nabla Z\mathcal{F}) &= \begin{vmatrix} \frac{\partial\mathcal{F}}{\partial u} & \frac{\partial Z\mathcal{F}}{\partial u} \\ \frac{\partial\mathcal{F}}{\partial v} & \frac{\partial Z\mathcal{F}}{\partial v} \end{vmatrix} \\ &= A(C^2M + 2CMu + (2M + C(1 - 3C + M))u^2 - 8Cu^3 - 4u^4) \\ &\quad + C^2((3 + 3M - 8u)u^2 + v) + 2u^2((2 + 2M - 5u)u^2 + v) \\ &\quad + Cu(-u(M - 8(1 + M)u + 19u^2) + 2v).\end{aligned}$$

These terms will be used shortly. It follows from [4, Theorem 1] that

$$\begin{aligned}\mathcal{G}(u, v) &= \det(\mathcal{Q}, Z) \cdot \det(\nabla\mathcal{F}, \nabla Z\mathcal{F}) \\ &= -\left((A + u)v(u - Qv + C)(A(C^2M + 2CMu \right. \\ &\quad \left. + (2M + C(1 - 3C + M))u^2 - 8Cu^3 - 4u^4) + C^2((3 + 3M - 8u)u^2 + v) \right. \\ &\quad \left. + 2u^2((2 + 2M - 5u)u^2 + v) + Cu(-u(M - 8(1 + M)u + 19u^2) + 2v)\right),\end{aligned}$$

and one obtains the value

$$\begin{aligned}\mathcal{A}(u, v) &= \frac{ZZZ\mathcal{F}(u, v)}{[ZZ\mathcal{F}(u, v)]^2} \\ &= \frac{3}{\Lambda} \left[(-M + C(1 + M - 4u) + A(1 - C + M - 4u) + 4u + 4Mu - 10u^2) \right],\end{aligned}$$

where

$$\begin{aligned}\Lambda &= 2(-3Mu + 6u^2 + 6Mu^2 - 10u^3 + C(-M + 3u + 3Mu - 6u^2) \\ &\quad + A(-M + C(1 + M - 3u) + 3u + 3Mu - 6u^2) - v)^2.\end{aligned}$$

Now, we define $\mathcal{V} = a_1 \frac{\partial}{\partial u} + a_2 \frac{\partial}{\partial v}$, where a_1 and a_2 are arbitrary functions to be determined. The next step is to see that the conditions for a slow-fast Hopf point are satisfied and also to use the intrinsically defined vector field \mathcal{V} with which we will provide the formula for the criticality.

First, we should find a_1 and a_2 as the solution to the system of equations $\mathcal{V}(\mathcal{F}) = 0$ and $\mathcal{V}(Z\mathcal{F}) = 1$. In doing that we obtain

$$\mathcal{V} = \frac{-\frac{\partial \mathcal{F}}{\partial v}}{\det(\nabla \mathcal{F}, \nabla Z\mathcal{F})} \frac{\partial}{\partial u} + \frac{\frac{\partial \mathcal{F}}{\partial u}}{\det(\nabla \mathcal{F}, \nabla Z\mathcal{F})} \frac{\partial}{\partial v}. \quad (29)$$

We remark that according to [4], this solution is uniquely defined. Let us next compute

$$\begin{aligned}\mathcal{V}\mathcal{F}(u, v) &= \frac{-\frac{\partial \mathcal{F}}{\partial v}}{\det(\nabla \mathcal{F}, \nabla Z\mathcal{F})} \frac{\partial}{\partial u} \mathcal{F} + \frac{\frac{\partial \mathcal{F}}{\partial u}}{\det(\nabla \mathcal{F}, \nabla Z\mathcal{F})} \frac{\partial}{\partial v} \mathcal{F}, \\ \mathcal{V}\mathcal{G}(u, v) &= \frac{-\frac{\partial \mathcal{F}}{\partial v}}{\det(\nabla \mathcal{F}, \nabla Z\mathcal{F})} \frac{\partial}{\partial u} \mathcal{G} + \frac{\frac{\partial \mathcal{F}}{\partial u}}{\det(\nabla \mathcal{F}, \nabla Z\mathcal{F})} \frac{\partial}{\partial v} \mathcal{G}, \\ \mathcal{V}^2\mathcal{G}(u, v) &= \frac{-\frac{\partial \mathcal{F}}{\partial v}}{\det(\nabla \mathcal{F}, \nabla Z\mathcal{F})} \frac{\partial}{\partial u} \mathcal{V}\mathcal{G} + \frac{\frac{\partial \mathcal{F}}{\partial u}}{\det(\nabla \mathcal{F}, \nabla Z\mathcal{F})} \frac{\partial}{\partial v} \mathcal{V}\mathcal{G}.\end{aligned}$$

One can confirm that as required by [4, Theorem 2], we have

$$\mathcal{G}|_{Q=Q_H(P)} = 0, \quad \mathcal{V}|_{Q=Q_H(P)}(\mathcal{G}|_{Q=Q_H(P)}) < 0, \quad \frac{\partial}{\partial Q}\mathcal{G}|_{Q=Q_H(P)} \neq 0. \quad (30)$$

Combining these equations, we find

$$\sigma = \frac{1}{2} \mathcal{V}^2\mathcal{G}(u_p, v_p) - \mathcal{V}\mathcal{G}(u_p, v_p) \mathcal{A}(u_p, v_p). \quad (31)$$

For our particular model, determining analytically the sign of σ is unfeasible due to its complexity. However, we present representative slices of the graph of $\sigma = \sigma(A, C, M)$ given by (31) in Figure 8, where it is evident that both regimes, super- and sub- critical exist. Nevertheless, the previous analysis proves the following proposition, which is specialized to the purposes of the paper.

Proposition 3. *There exists an open set of parameter values (A, M, C) with $A \approx \frac{1}{2}$ and $M \approx -\frac{1}{10}$ for which (16) undergoes a supercritical Hopf bifurcation at $Q = Q_H$.*

Remark 7. *The numerical values $A = \frac{1}{2}$ and $M = -\frac{1}{10}$ are chosen simply for purposes of simulations. One can compare and complement this with Figure 17.*

Now that we have determined that the point P is a singular supercritical Hopf point, we proceed with the other singular point, which is the point T_C under the condition that $C = -AMQ$.

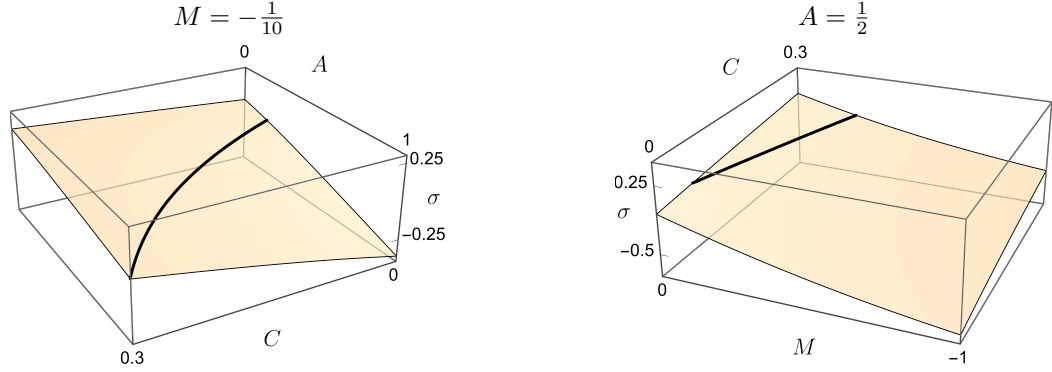


FIGURE 8. We present slices of (31) for the indicated values of parameters. In this way, we verify the region of parameters for which the Hopf bifurcation is super- ($\sigma < 0$) or sub- ($\sigma > 0$) critical. The black curve indicates $\sigma = 0$.

6. DESINGULARIZATION OF THE POINT T_C , IN THE DEGENERATE CASE $C = -AMQ$

In this section, we provide a local analysis of the system near the point T_C for the degenerate scenario $C = -AMQ$, recall Figure 4. For convenience, we rewrite the system under consideration, namely

$$X : \begin{cases} \frac{du}{dt} = u(u - AMQ)(AM - (u - M)(u - 1)(A + u) - v), \\ \frac{dv}{dt} = \varepsilon(u + A)(v - AM)(u - Qv), \\ \frac{d\varepsilon}{dt} = 0, \end{cases} \quad (32)$$

where we have also shifted the origin to the point T_C , recycled the coordinates, and added the trivial equation $\frac{d\varepsilon}{dt} = 0$. A simple computation confirms that the origin is nilpotent. Thus, we propose a blow-up of the form

$$(u, v, \varepsilon) = (r\bar{u}, r\bar{v}, r\bar{\varepsilon}), \quad (33)$$

where $\bar{u}^2 + \bar{v}^2 + \bar{\varepsilon}^2 = 1$ and $r \in [0, r_0)$. Details of the blow-up transformation can be found in [19] and references therein. As usual, we will study several local vector fields on different charts of the blow-up space. These charts and the corresponding local coordinates are introduced below.

For reasons that become clear in the blow-up analysis, we introduce the non-degeneracy conditions $A - M + AM \neq 0$ and $A - M + AM \neq \frac{1}{Q}$.

6.1. Entry chart. The local coordinates in this chart $K_1 = \{\bar{v} = 1\}$ are given by

$$u = r_1 u_1, \quad v = r_1, \quad \varepsilon = r_1 \epsilon_1, \quad (34)$$

which leads to the local vector field

$$\begin{aligned}\frac{dr_1}{dt_1} &= r_1 \epsilon_1 (Q - u_1) (A^2 M + \mathcal{O}(r_1)), \\ \frac{du_1}{dt_1} &= AMQ(1 - (A + M - AM)u_1)u_1 - A^2 M(Q - u_1)u_1 \epsilon_1 + \mathcal{O}(r_1), \\ \frac{d\epsilon_1}{dt_1} &= -\epsilon_1^2 (Q - u_1) (A^2 M + \mathcal{O}(r_1)),\end{aligned}\tag{35}$$

where t_1 denotes the time in this chart (after blow-up and desingularization).

In this chart, we are first interested in the restriction of (35) to $r_1 = 0$, which reads as:

$$\begin{aligned}\frac{du_1}{dt_1} &= AMQ(1 - (A + M - AM)u_1)u_1 - A^2 M(Q - u_1)u_1 \epsilon_1, \\ \frac{d\epsilon_1}{dt_1} &= -A^2 M \epsilon_1^2 (Q - u_1).\end{aligned}\tag{36}$$

Proposition 4. *The origin is a semi-hyperbolic equilibrium point of (36) and has a unique 1-dimensional, locally attracting, center manifold \mathcal{M}_1 associated to it. For $\epsilon_1 \geq 0$, \mathcal{M}_1 is unique, coincides with the ϵ_1 -axis, and the flow along it is directed away from the origin.*

Remark 8. *System (36) has another equilibrium point at $(u_1, \epsilon_1) = \left(\frac{1}{A-M+AM}, 0\right)$ but this is studied in the chart K_3 .*

Proof. The statements follow from standard center manifold arguments. We simply mention that the Jacobian at the origin is

$$J = \begin{bmatrix} AMQ & 0 \\ 0 & 0 \end{bmatrix},\tag{37}$$

and recall that $M < 0$. □

Next, the dynamics of (35) restricted to $\epsilon_1 = 0$ are given by:

$$\begin{aligned}\frac{dr_1}{dt} &= 0, \\ \frac{du_1}{dt} &= -AMQ(-1 + (A - M + AM)u_1)u_1 + O(r_1 u_1),\end{aligned}\tag{38}$$

for which it is straightforward to see that the r_1 -axis is a set of locally attracting equilibria.

Remark 9. *Notice that in this chart $\varepsilon = r_1 \epsilon_1$. Therefore, rescaling time, it is possible to readily see from (35) that the slow flow along the r_1 axis is given by $r_1' = A^2 M Q < 0$. See Figure 9.*

Let the sections Δ_1^{in} and Δ_1^{out} (see Figure 9) be defined as follows:

$$\begin{aligned}\Delta_1^{\text{in}} &= \{(r_1, u_1, \epsilon_1) : r_1 = \delta_1, 0 \leq u_1 < \tilde{u}_1, 0 \leq \epsilon_1 < \delta_2\} \\ \Delta_1^{\text{out}} &= \{(r_1, u_1, \epsilon_1) : \epsilon_1 = \delta_2, 0 \leq u_1 < \tilde{u}_1, 0 \leq r_1 < \delta_1\},\end{aligned}\tag{39}$$

with δ_1 , δ_2 , and \tilde{u}_1 sufficiently small constants. Let $\Pi_1 : \Delta_1^{\text{in}} \rightarrow \Delta_1^{\text{out}}$ be defined by the flow of (35). From the analysis performed above, the next characterization of the map Π_1 follows:

Proposition 5. *The map Π_1 is well-defined and is, moreover, a contraction. In particular, the image of Δ_1^{in} under Π_1 is a wedge-like region contained in Δ_1^{out} .*

The flow in this chart near the origin is sketched in Figure 9.

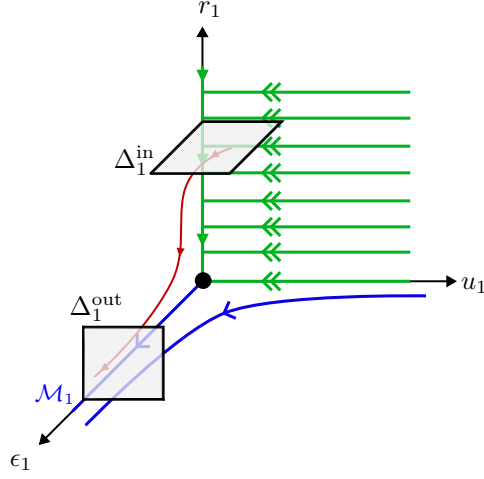


FIGURE 9. Following the analysis presented in this section, we provide a sketch of the dynamics of (35) near the origin. The limit dynamics are presented in green and blue (for $\epsilon_1 = 0$ and $r_1 = 0$ respectively), while a sample orbit of (35) is shown in red.

6.2. **Central chart.** The local coordinates in this chart $K_2 = \{\bar{\epsilon} = 1\}$ are given by

$$u = r_2 u_2, \quad v = r_2 v_2, \quad \epsilon = r_2, \quad (40)$$

which leads to the local vector field

$$\begin{aligned} \frac{dr_2}{dt_2} &= 0 \\ \frac{du_2}{dt_2} &= -u_2(AMQ - ru_2)(Au_2(M - r_2u_2 + 1) + u_2(r_2u_2 - 1)(M - r_2u_2) - v_2) \\ \frac{dv_2}{dt_2} &= -((A + r_2u_2)(u_2 - Qv_2)(AM - r_2v_2)). \end{aligned} \quad (41)$$

Restricting to $\{r_2 = 0\}$ for (41), we focus on

$$\begin{aligned} \frac{du_2}{dt_2} &= -AMQu_2((A - M + AM)u_2 - v_2), \\ \frac{dv_2}{dt_2} &= -A^2M(u_2 - Qv_2), \end{aligned} \quad (42)$$

where, since now r_2 is a regular parameter, the analysis that follows provides the qualitative dynamics also for r_2 sufficiently small.

Proposition 6. *The following statements hold for (42):*

- (1) *The origin is the unique equilibrium point, and the v_2 -axis is invariant under the flow. Moreover, the flow along the v_2 -axis is directed towards the origin.*
- (2) *The origin is semi-hyperbolic. For $u_2 \geq 0$, there exists a locally attracting 1-dimensional center manifold \mathcal{M}_2 tangent, at the origin, to the center eigenspace $E^c = \text{span} \left\{ \begin{bmatrix} Q \\ 1 \end{bmatrix} \right\}$.*

(3) For $u_2 \geq 0$: a) if $A - M + AM < \frac{1}{Q}$ then the origin is locally stable; b) if $A - M + AM > \frac{1}{Q}$ then the origin is unstable and the center manifold is unique.

Proof. The first two items are straightforward. For the third, let $\mathcal{M}_2 = \{(u_2, v_2) \in \mathbb{R}^2 \mid v_2 = h_2(u_2)\}$, with $h_2(0) = 0$ and $\frac{dh_2}{du_2}(0) = \frac{1}{Q}$. Standard center manifold computations lead to

$$h_2(u_2) = \frac{1}{Q}u_2 + \frac{1 - (A - M + AM)Q}{AQ^2}u_2^2 + \mathcal{O}(u_2^3), \quad (43)$$

which implies that

$$\left. \frac{du_2}{dt_2} \right|_{\mathcal{M}_2} = -AMQ(A - M + AM - \frac{1}{Q})u_2^2 + \mathcal{O}(u_2^3), \quad (44)$$

leading to the statement (we recall that $M < 0$). The reason why the center manifold is unique in the case $A - M + AM - \frac{1}{Q} > 0$ is due to the saddle-like behavior near the origin. \square

We are further interested in the case where the flow on the center manifold \mathcal{M}_2 goes away from the origin because this will help us prove the possibility of relaxation oscillations in the degenerate setting $C = -AMQ$. So, let us define the sections:

$$\begin{aligned} \Delta_2^{\text{in}} &= \{(u_2, v_2) : 0 \leq u_2 < \tilde{u}_2, v_2 = \delta_3\}, \\ \Delta_2^{\text{out}} &= \{(u_2, v_2) : u_2 = \delta_4, |v_2 - h_2(\delta_4)| < \delta_5\}, \end{aligned} \quad (45)$$

where $\tilde{u}_2, \delta_3, \delta_4, \delta_5$ are all positive small constants further satisfying $\tilde{u}_2 < \delta_4$ and $h(\delta_4) + \delta_5 < \delta_3$. Let $\Pi_2 : \Delta_2^{\text{in}} \rightarrow \Delta_2^{\text{out}}$ be defined by the flow of (42). The following proposition characterizes Π_2 .

Proposition 7. *Let $A - M + AM - \frac{1}{Q} > 0$ and \tilde{u}_2 sufficiently small. The map Π_2 is well-defined. In particular, within a small neighborhood of \mathcal{M}_2 , the flow of (42) contracts towards \mathcal{M}_2 .*

Proof. The statements follow from proposition 6 and standard center manifold arguments. In particular, let $e = v_2 - h$. It follows that:

$$\begin{aligned} \frac{de}{dt_2} &= \frac{dv_2}{dt_2} - \frac{\partial h_2}{\partial u_2} \frac{du_2}{dt_2} \\ &= -A^2M(u_2 - Q(e + h_2)) - \frac{\partial h_2}{\partial u_2} \frac{du_2}{dt_2} \\ &= A^2QMe + A^2M(Qh_2 - u_2) - \frac{\partial h_2}{\partial u_2} \frac{du_2}{dt_2} \\ &= A^2QMe, \end{aligned} \quad (46)$$

where the last equality follows from the invariance of $\mathcal{M}_2 = \{v_2 = h_2(u_2)\}$. Recall that $M < 0$. \square

We notice that Proposition 7 shows that, under the setting of the proposition, the center manifold \mathcal{M}_2 is locally attracting everywhere and not only close to the origin.

The flow of (42) is sketched in Figure 10. We recall that in this chart, $r_2 = \varepsilon$ is a regular perturbation parameter.

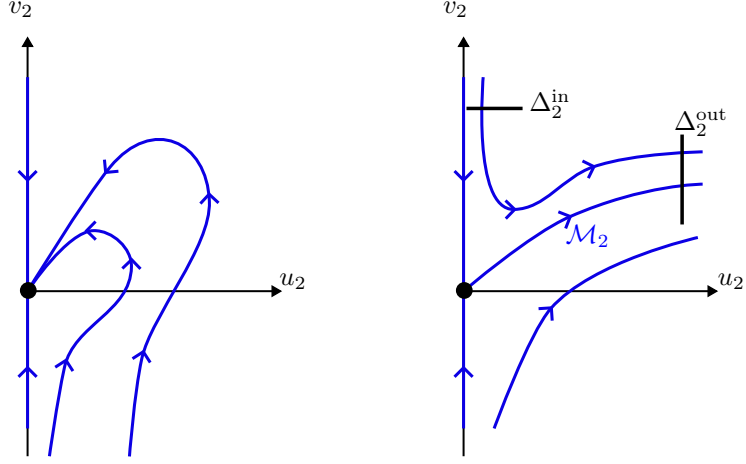


FIGURE 10. Phase-portrait of (42) for $A - M + AM - \frac{1}{Q} < 0$ on the left and $A - M + AM - \frac{1}{Q} > 0$ on the right. The phase portraits are drawn qualitatively by exploiting Proposition 6, the fact that $\frac{dv_2}{dt} > 0$ for all $v_2 < 0$ and the relative arrangement of the nullclines $v_2 = (A - M + AM)u_2$, where we recall that $A - M + AM > 0$, and $v_2 = \frac{1}{Q}u_2$.

6.3. **Exit Chart.** The local coordinates in this chart $K_3 = \{\bar{u} = 1\}$ are given by

$$u = r_3, \quad v = r_3 v_3, \quad \varepsilon = r_3 \varepsilon_3, \quad (47)$$

which leads to the local vector field

$$\begin{aligned} \frac{dr_3}{dt_3} &= -AMQr_3(A - M + AM - v_3) \\ &\quad + (A - M + AM - AMQ + A^2MQ - AM^2Q - v_3)r_3^2 + \mathcal{O}(r_3^3), \\ \frac{dv_3}{dt_3} &= AMQ(A - M + AM - v_3)v_3 + A^2M(Qv_3 - 1)\varepsilon_3 + \mathcal{O}(r_3), \\ \frac{d\varepsilon_3}{dt_3} &= AMQ\varepsilon_3(A - M + AM - v_3) + \mathcal{O}(\varepsilon_3 r_3), \end{aligned} \quad (48)$$

where t_3 denotes the rescaled time in this chart and $r_3 \geq 0$, $\varepsilon_3 \geq 0$. First, we consider (48) restricted to $r_3 = 0$, that is:

$$\begin{aligned} \frac{dv_3}{dt_3} &= AMQ(A - M + AM - v_3)v_3 + A^2M(Qv_3 - 1)\varepsilon_3, \\ \frac{d\varepsilon_3}{dt_3} &= AMQ\varepsilon_3(A - M + AM - v_3). \end{aligned} \quad (49)$$

Proposition 8. *The following statements hold for (49) (recall that $A - M + AM > 0$):*

(1) *There are two equilibrium points:*

$$o_3 = (0, 0) \quad \text{and} \quad p_3 = (A - M + AM, 0). \quad (50)$$

- (2) The equilibrium point o_3 is a hyperbolic sink.
(3) The equilibrium point p_3 is semi-hyperbolic and has a 1-dimensional locally repelling center manifold \mathcal{N}_3 associated to it. If in addition $A - M + AM < \frac{1}{Q}$ then the flow along \mathcal{N}_3 is directed towards p_3 and \mathcal{N}_3 is unique; on the other hand, if $A - M + AM > \frac{1}{Q}$ then the flow along \mathcal{N}_3 is directed away from p_3 .

Proof. The first two statements are straightforward. For the third, standard center manifold computations show that $\mathcal{N}_3 = \{(v_3, \epsilon_3) \in \mathbb{R}^2 \mid v_3 = g_3(\epsilon_3)\}$ is given by

$$g_3(\epsilon_3) = A - M + AM + \frac{A(A - M + AM - \frac{1}{Q})}{(A - M + AM)Q} \epsilon_3 + \frac{A^2(A - M + AM - \frac{1}{Q})}{(A - M + AM)Q^2} \epsilon_3^2 + \mathcal{O}(\epsilon_3^3), \quad (51)$$

which implies that

$$\left. \frac{d\epsilon_3}{dt_3} \right|_{\mathcal{N}_3} = -\frac{A^2 M (A - M + AM - \frac{1}{Q})}{(A - M + AM)} \epsilon_3^2 + \mathcal{O}(\epsilon_3^3), \quad (52)$$

leading to the statement (we recall that $M < 0$). The uniqueness of the center manifold follows from the saddle-like behavior in the corresponding case. \square

Remark 10. The center manifold \mathcal{M}_2 in chart K_2 is contained in the forward invariant set $\Gamma_2 = \{(u_2, v_2) \in \mathbb{R}^2 \mid u_2 > 0, 0 < v_2 < \frac{1}{Q} u_2\}$. In the coordinates of chart K_3 , Γ_2 corresponds to $\Gamma_3 = \{(\epsilon_3, v_3) \in \mathbb{R}^2 \mid 0 < v_3 < \frac{1}{Q}\}$. It then follows from Proposition 8 that for $A - M + AM > \frac{1}{Q}$, the unique center manifold \mathcal{M}_2 converges to the origin of chart K_3 . In this setting, let us denote by \mathcal{M}_3 a parametrization of \mathcal{M}_2 in the coordinates of K_3 and assume that (at least locally) $\mathcal{M}_3 = \{v_3 = h_3(\epsilon_3)\}$.

On the other hand, system (48) restricted to $\epsilon_3 = 0$ is given by:

$$\begin{aligned} \frac{dr_3}{dt_3} &= -(AMQ - r_3)(A(1 + M - r_3) + (M - r_3)(r_3 - 1) - v_3)r_3, \\ \frac{dv_3}{dt_3} &= (AMQ - r_3)(A(1 + M - r_3) + (M - r_3)(r_3 - 1) - v_3)v_3, \end{aligned} \quad (53)$$

where we recall that $r_3 \geq 0$.

Proposition 9. The following statements hold for (53) (recall that $A - M + AM > 0$):

- (1) The origin $o_3 = (0, 0)$ is a hyperbolic saddle. In particular, the r_3 -direction is repelling while the v_3 -direction is attracting.
(2) There is a curve of equilibria

$$\ell_3 = \{(r_3, v_3) \in \mathbb{R}^2 \mid v_3 = A - M + AM + (1 - A + M)r_3 - r_3^2\}. \quad (54)$$

For r_3 sufficiently small, the curve ℓ_3 is repelling.

Proof. All statements are straightforward. We indicate that the nontrivial eigenvalue along ℓ_3 is $\lambda = -AMQ(A - M + AM) + \mathcal{O}(r_3)$ and recall that $M < 0$. \square

Remark 11. It follows by substituting $(u, v) = (r_3, r_3 v_3)$ into the expression of the critical manifold of (32), that the curve ℓ_3 is, in fact, the critical manifold \mathcal{M}_0^1 written in the coordinates of chart K_3 .

Proposition 10. *Let $A - M + AM - \frac{1}{Q} > 0$. There is a (non-unique) 2-dimensional center manifold \mathcal{P}_3 at the point p_3 . The flow restricted to it is of saddle type, with the direction r_3 stable, and the direction ϵ_3 unstable, as sketched in Figure 11.*

Proof. The result follows from standard center manifold computations, so we simply report the important steps. Assuming that the center manifold can be given as the graph of $v_3 = H_3(r_3, \epsilon_3)$, we find that

$$H_3 = A - M + AM + \frac{-1 + (A - M + AM)Q}{(A - M + AM)Q} A\epsilon_3 + (1 - A + M)r + O(r_3^2, \epsilon_3^2, r_3\epsilon_3). \quad (55)$$

The reduced dynamics on the center manifold are therefore given by

$$\begin{aligned} \frac{dr_3}{dt_3} &= \frac{r_3(AMQ - r_3)(A\epsilon_3(-1 + (A - M + AM)Q) + (A - M + AM)Qr^2)}{(A - M + AM)Q} \\ \frac{d\epsilon_3}{dt_3} &= -\frac{\epsilon_3(AMQ - r_3)(A\epsilon_3(-1 + (A - M + AM)Q) + (A - M + AM)Qr^2)}{(A - M + AM)Q}. \end{aligned} \quad (56)$$

The condition $A - M + AM - \frac{1}{Q} > 0$, together with $M < 0$ and $A - M + AM > 0$, imply that the common term $\frac{A\epsilon_3(-1 + (A - M + AM)Q) + (A - M + AM)Qr^2}{(A - M + AM)Q}$ is positive. The statement hence follows. \square

We now describe the two most important transition maps. Let us define the sections:

$$\begin{aligned} \Delta_3^{\text{in}} &= \{(r_3, v_3, \epsilon_3) : \epsilon_3 = \delta_6, |v_3 - h_3(\delta_6)| < \delta_7, 0 \leq r_3 < \tilde{r}_3\}, \\ \Delta_c^{\text{in}} &= \{(r_3, v_3, \epsilon_3) : r_3 = \rho_3, |v_3 - \ell_3| < e^{-c/\epsilon}, 0 \leq \epsilon_3 < \delta_8\} \\ \Delta_3^{\text{out}} &= \{(r_3, v_3, \epsilon_3) : r_3 = \delta_9, |v_3| < \delta_{10}, 0 \leq \epsilon_3 < \tilde{\epsilon}_3\}, \end{aligned} \quad (57)$$

where all the introduced constants are sufficiently small and positive, further satisfying $\tilde{\epsilon}_3 < \delta_6$, $\tilde{r}_3 < \delta_9$, $\delta_8 < \delta_6$. Let the maps $\Pi_3 : \Delta_3^{\text{in}} \rightarrow \Delta_3^{\text{out}}$ and $\Pi_3^c : \Delta_c^{\text{in}} \rightarrow \Delta_3^{\text{out}}$ be defined by the flow of (48). The analysis presented above suffices to show the following:

Proposition 11.

- The map Π_3 is well defined. In particular, the image of Δ_3^{in} under the map Π_3 is a wedge-like region contained in Δ_3^{out} and Π_3 is an exponential contraction towards the r_3 -axis.
- The map Π_3^c is well defined. The image of the exponentially thin strip Δ_c^{in} is an exponentially thin strip contained in Δ_3^{out} .

The dynamics in this chart, following Propositions 8, 9, 10 and 11, are summarized in Figure 11.

For completeness, we briefly present the dynamics on the bottom chart in the following section.

6.4. Bottom chart. The local coordinates in this chart $K_4 = \{\bar{v} = -1\}$ are given by

$$u = r_4 u_4, \quad v = -r_4, \quad \varepsilon = r_4 \epsilon_4, \quad (58)$$

which leads to the local vector field

$$\begin{aligned} \frac{dr_4}{dt} &= r_4 \epsilon_4 (Q + u_1) (A^2 M + \mathcal{O}(r_4)), \\ \frac{du_4}{dt} &= -AMQ(1 + (A + M - AM)u_4)u_4 - A^2 M(Q + u_4)u_4 \epsilon_4 + \mathcal{O}(r_4), \\ \frac{d\epsilon_4}{dt} &= -\epsilon_4^2 (Q + u_4) (A^2 M + \mathcal{O}(r_4)). \end{aligned} \quad (59)$$

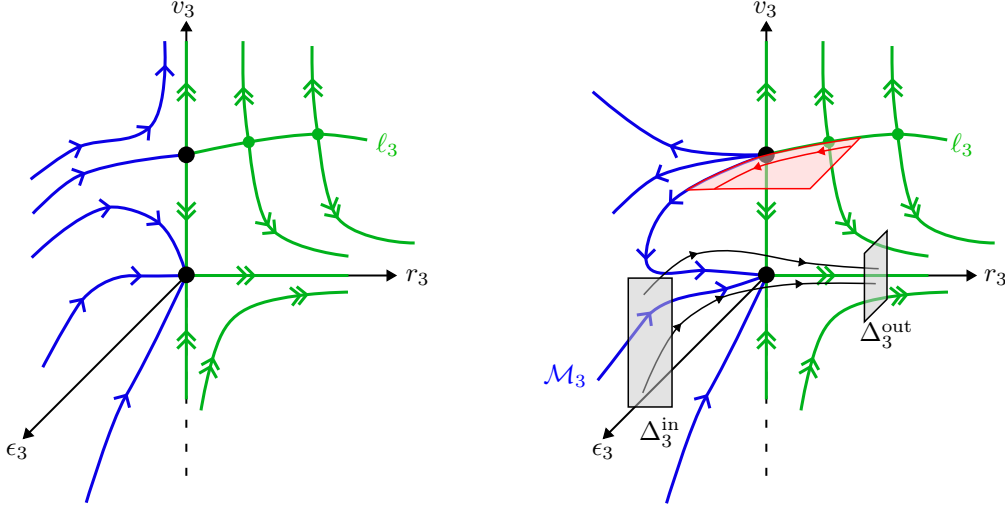


FIGURE 11. Dynamics of (35) in the chart $K_3 = \{\bar{u} = 1\}$ for $A - M + AM - \frac{1}{Q} < 0$ on the left and $A - M + AM - \frac{1}{Q} > 0$ on the right. The flow in blue occurs in the (ϵ_3, v_3) -plane, while the green one in the (r_3, v_3) -plane. The black orbits are a sketch of a sample of orbits flowing from Δ_3^{in} and arriving at Δ_3^{out} . The red surface is the center manifold \mathcal{P}_3 . Notice that since ℓ_3 is simply the critical manifold \mathcal{M}_0^1 written in the local coordinates of this chart, the orbits on \mathcal{P}_3 can be identified with the slow manifolds that perturb from \mathcal{M}_0^1 . Although we do not show Δ_c^{in} , as it is an exponentially thin strip, it is evident from the analysis presented that some of the orbits near \mathcal{P}_3 arrive at Δ_3^{out} .

The dynamics are similar to that on the entry chart, just with the ε -direction reversed, so we simply show in Figure 12 the corresponding flow and omit the details.

6.5. Blown-up dynamics at T_C , relaxation oscillations, and transitory canard. With the analysis performed in sections 6.1-6.4 we deduce that the blown-up dynamics at T_C are given by two non-equivalent flows as shown in Figure 13.

In particular, the proof of the following proposition follows from the analysis carried out previously.

Proposition 12. *Consider system (32) and let Σ_0 , Σ_1 , and Σ_2 be sections defined as follows (refer also to Figure 13):*

$$\begin{aligned} \Sigma_0 &= \{(u, v, \varepsilon) \in \mathbb{R}^3 : 0 \leq u < \tilde{u}, v = \tilde{v}, \varepsilon \ll 1\} \\ \Sigma_1 &= \{(u, v, \varepsilon) \in \mathbb{R}^3 : u = u^*, h(u) - \delta \leq v < h(u) + \delta, \varepsilon \ll 1\} \\ \Sigma_2 &= \{(u, v, \varepsilon) \in \mathbb{R}^3 : u = u^*, 0 \leq v < h(u), \varepsilon \ll 1\}, \end{aligned} \quad (60)$$

where $\tilde{u} < u^* < u^*$ are sufficiently small positive constants. Then, for $A - M + AM > \frac{1}{Q}$ and $\varepsilon > 0$ sufficiently small:

- The map $\Pi_{0 \rightarrow 2} : \Sigma_0 \mapsto \Sigma_2$ induced by the flow of (32) is well defined and is a contraction.

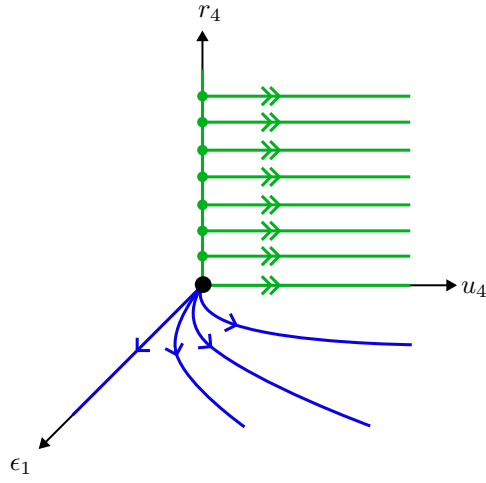


FIGURE 12. Dynamics of (59) near the origin. In contrast to the flow of (35), the center manifold in the plane (v_4, ϵ_4) is not unique.

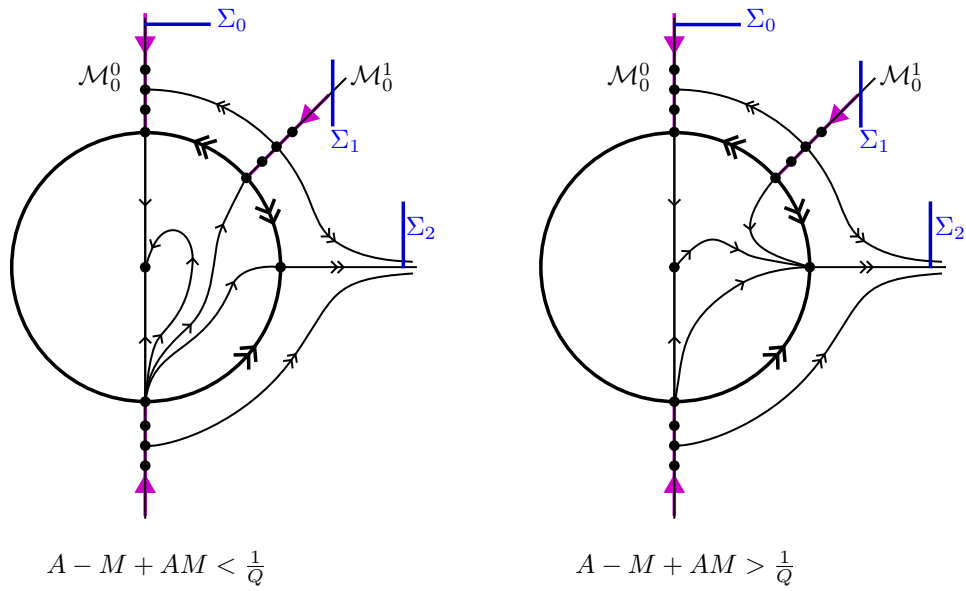


FIGURE 13. The two non-equivalent blown-up dynamics of the point T_C for $A - M + AM < \frac{1}{Q}$ on the left and $A - M + AM > \frac{1}{Q}$ on the right. The dotted curves depict the critical manifold. The corresponding reduced flows are indicated by the magenta arrows. Compare with figure 4 near the point T_C .

- For $\delta > 0$ exponentially small and $Q = Q_m \sim Q_H$ as $\varepsilon \rightarrow 0$, where Q_m is the value of the parameter Q for which there is a maximal canard at P , the map $\Pi_{1 \rightarrow 2} : \Sigma_1 \mapsto \Sigma_2$ induced by the flow of (32) is well defined.

Proof. At the singular level, i.e. for $\varepsilon = 0$, the map $\Pi_{0 \rightarrow 2}$ is described by the concatenation of the corresponding orbits for $\bar{r} = 0$ in the blow-up analysis performed in Sections 6.1-6.4, refer in particular Figures 9, 10 and 11 and the analysis leading to them, together with a blow-down. For the map $\Pi_{1 \rightarrow 2}$ one just needs to be careful to have the appropriate parameters such that the slow flow along $\mathcal{M}_0^{1,r}$ is directed towards T_C as in Figure 7 and that the parameter Q is chosen so that there is a maximal canard at the fold point P . This is achieved for parameters exponentially close to $Q = Q_H$. Since we have already shown in Section 5 that the singular Hopf bifurcation at P for $Q = Q_H$ may be supercritical, the appropriate choice of parameters guarantee that such a maximal canard is stable for $\varepsilon > 0$ sufficiently small. \square

Remark 12. For $A - M + AM < \frac{1}{Q}$, one can show that trajectories that cross Σ_0 transversally converge to the origin. Since this does not lead to oscillatory behavior, we do not detail this case anymore. It is nevertheless interesting to observe that, in this case, the degenerate point T_C is a saddle but eventually attracts all orbits.

Next, we discuss oscillations that are organized by the two singularities, the fold P and the degenerate saddle T_C , see figure 14, which is now presented in the original coordinates (u, v) of system (2) where $S = \varepsilon$.

We have all the elements to prove the following:

Theorem 4. Consider system (2) and let $C = -AMQ$ and $A - M + AM > \frac{1}{Q}$.

- (1) Let the parameters $(A, M, Q) \in (0, 1) \times (-1, 0) \times \mathbb{R}_{>0}$ be chosen such that the fold point P is a generic jump point. In particular, this implies that the equilibrium point $E_1 = (\mathcal{U}_1, \mathcal{V}_1)$ is on the left branch of \mathcal{M}_0^1 with $0 < \mathcal{U}_1 < u_p$. Assume that E_1 lies within a distance of order $\mathcal{O}(1)$ from either singularity T_C and P . For $\varepsilon = 0$, there is a singular orbit γ_0 as shown in the left panel of Figure 14. For $S = \varepsilon \ll 1$ there is a locally stable cycle γ_ε that converges in Hausdorff distance to γ_0 as $\varepsilon \rightarrow 0$.
- (2) Let the parameters $(A, M, Q) \in (0, 1) \times (-1, 0) \times \mathbb{R}_{>0}$ be chosen such that the fold point P is a canard point, i.e. $Q = Q_H$, where Q_H was given in (15). For $\varepsilon = 0$, there is a singular orbit $\tilde{\gamma}_0$ as shown in the right panel of Figure 14. For $S = \varepsilon \ll 1$ and $Q = Q_c(\varepsilon) \approx Q_H$ where Q_c is the value of the parameter Q for which a maximal canard exists, there is a locally stable cycle $\tilde{\gamma}_\varepsilon$ that converges in Hausdorff distance to $\tilde{\gamma}_0$ as $\varepsilon \rightarrow 0$.

Proof. We refer to suitably defined sections as shown in Figure 14. For both cases, the transition $\Sigma_2 \rightarrow \Sigma_3$ follows from Fenichel's theory, as does $\Sigma_4 \rightarrow \Sigma_0$. In addition, such transitions are exponential contractions. The transitions $\Sigma_3 \rightarrow \Sigma_4$, which is also a contraction, and $\Sigma_3 \rightarrow \Sigma_1$ follow from [21]. The transitions $\Sigma_0 \rightarrow \Sigma_2$ and $\Sigma_1 \rightarrow \Sigma_2$ are both contractions and are the blow-down versions of Proposition 12. Hence, the existence and stability of γ_ε and of $\tilde{\gamma}_\varepsilon$ follow from the concatenation of the aforementioned maps. \square

To finish this section, we present in Figure 15 a sample of numerical simulations representative of Theorem 4. To have a clearer impression of the values of bifurcation parameter Q we chose its values as $Q = Q_H - \delta$, where the corresponding value of δ appears at the top of each figure.

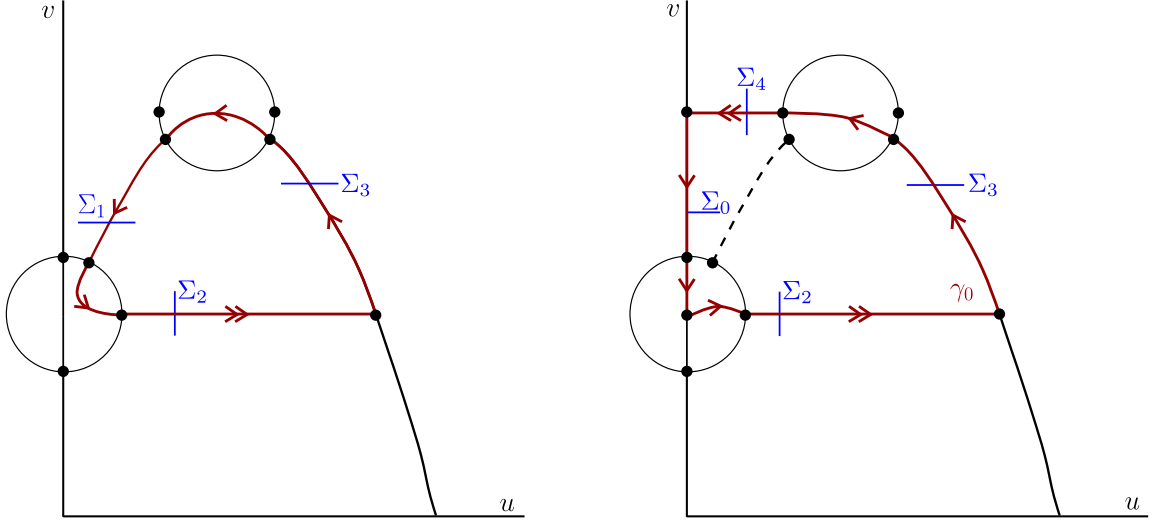


FIGURE 14. On the left we show we show a transitory canard passing through the fold point P and the singular point T_C . On the right, a singular relaxation oscillations passing through the same singularities. These cycles are obtained for different parameter regimes (recall that in this section $C = -AMQ$) provided that $A - M + AM > \frac{1}{Q}$. The relaxation oscillation is obtained when the fold point P is a generic jump point. The transitory canard is obtained when the fold point undergoes a singular Hopf bifurcation and the parameter $Q \approx Q_H$ is chosen so that there is a maximal canard at P .

7. RELAXATION OSCILLATIONS FOR $C < -AMQ$

In Section 6, we have studied dynamics organized by a singular Hopf bifurcation and a degenerate transcritical point, T_C . In this section, we consider the case where T_C is instead a generic transcritical point. The advantage is that, in this case, one can study the transition across T_C using the entry-exit function [6], which is not possible in the degenerate scenario. Moreover, we will show the existence of an orbit that jumps from the fold point to the other by attracting the slow manifold \mathcal{M}_0^0 through fast horizontal flow and continuing there for a constant time, the orbit leaves \mathcal{M}_0^0 at a certain point.

To do this, first, we restrict our attention to the system (2) written as follows

$$\begin{aligned} \frac{du}{dt} &= uf_1(u, v) = u((u + C)((u + A)(1 - u)(u - M) - v)), \\ \frac{dv}{dt} &= \varepsilon vg_1(u, v) = \varepsilon v(S(u + A)(u + C - Qv)). \end{aligned} \tag{61}$$

A straightforward calculation shows us that $f_1(0, v) = c(-AM - v)$, $g_1(0, v) = SA(C - Qv)$, which implies that $f_1(0, v) < 0$ if $v > -AM$, $f_1(0, v) > 0$ if $v < -AM$. $T_C(0, -AM)$ on the vertical axis is the transcritical bifurcation point and we can split the slow manifold \mathcal{M}_0^0 into two parts $\mathcal{M}_0^{0,a} = \{(u, v) : u = 0, v > -AM\}$ and $\mathcal{M}_0^{0,r} = \{(u, v) : u = 0, v < -AM\}$. Indeed, $\mathcal{M}_0^{0,a}$ is attracting and $\mathcal{M}_0^{0,r}$ is repelling.

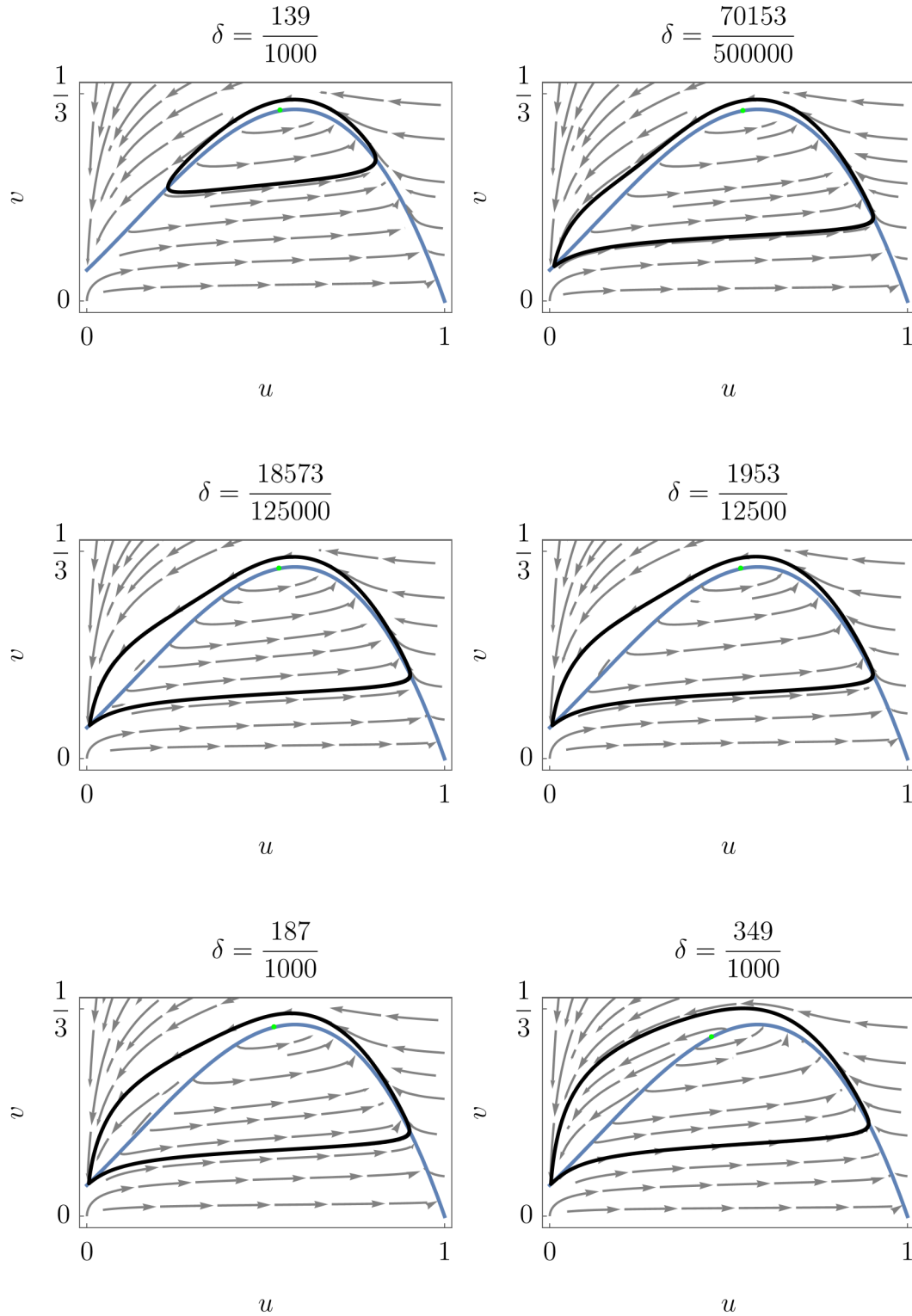


FIGURE 15. Simulations of (2) with $S = \varepsilon = 0.05$, $A = \frac{1}{2}$, $M = -\frac{1}{10}$, and $C = -AMQ$. The equilibrium point E_1 is located close to the fold point P . The parameter Q is chosen as $Q = Q_H - \delta$ where δ is shown at the top of each figure. Notice, indeed, the canard explosion occurring for the chosen parameters. We highlight that some of the canard cycles pass through the degenerate point T_C .

Let us set $\varepsilon = 0$ and let u_p be the maximum point of the critical manifold \mathcal{M}_0^1 , already given in (21), which we recall is

$$u_p = \frac{1}{3}(1 - A + M + \beta), \quad (62)$$

where $\beta = \sqrt{1 + A + A^2 - M + AM + M^2}$, and from the definition of \mathcal{M}_0^1 , it follows that

$$v_p = (u_p + A)(1 - u_p)(u_p - M). \quad (63)$$

Next we consider a trajectory starting from a point, say (u_1, v_p) , where $u_1 < u_p$. The trajectory is attracted towards the attracting manifold $\mathcal{M}_0^{0,a}$ and starts moving downward maintaining proximity to $\mathcal{M}_0^{0,a}$. It is to be expected that the trajectory would leave the vertical axis at the bifurcation point \mathcal{T}_C where it loses its stability, see [29]. The trajectory crosses the point \mathcal{T}_C and continues moving vertically downwards staying close to the repelling part $\mathcal{M}_0^{0,r}$, for a certain time, until it reaches a minimal population of predators $p(v_p)$ such that $0 < p(v_p) < -AM$. After leaving the slow manifold close to the point $p(v_p)$, the trajectory begins to move along a nearly horizontal segment and is attracted to the slow attractor manifold \mathcal{M}_1^a . This exit point is defined by an implicit function $p(v_p)$, called entry-exit function [6], given by the formula

$$I(p(v_p)) := \int_{p(v_p)}^{v_p} \frac{f_1(0, v)}{vg_1(0, v)} dv = 0.$$

Let define $v_0 = p(v_p)$, then we have

$$I(v_0) = \int_{v_0}^{v_p} \frac{C(-AM - v)}{v(SA(C - Qv))} dv = \frac{(AMQ + C)}{AQS} \ln \left(\frac{C - Qv_p}{C - Qv_0} \right) + \frac{M}{S} \ln \left(\frac{v_0}{v_p} \right). \quad (64)$$

Proposition 13. *For any v_p , there exists a unique $\frac{C}{Q} < v_0 < -AM$ such that $I(v_0) = 0$.*

Proof. We start by observing that $AMQ + C < 0$. Hence, it is obvious that $\lim_{v_0 \rightarrow \frac{C}{Q}^+} I(v_0) = -\infty$.

Since $-\frac{AM}{v_p}$ and $\frac{C - Qv_p}{C + AMQ}$ take values in the interval $(0, 1)$, one gets:

$$I(-AM) = \frac{(AMQ + C)}{AQS} \ln \left(\frac{C - Qv_p}{C + QAM} \right) + \frac{M}{S} \ln \left(\frac{-AM}{v_p} \right) > 0.$$

So that, the sign change guarantees that there is a zero of $I(v_0)$ somewhere in $(\frac{C}{Q}, -AM)$.

On the other hand, we have that $AM + v_0 < 0$ and $C - Qv_0 < 0$, which imply that

$$\frac{dI(v_0)}{dv_0} = \frac{C(AM + v_0)}{ASv_0(C - Qv_0)} > 0.$$

It follows that $I(v_0)$ is a continuous increasing function on $(\frac{C}{Q}, -AM)$.

From the previous analysis, we conclude that there is only one $p(v_0) \in (\frac{C}{Q}, -AM)$ such that $I(v_0) = 0$. \square

Note that if we substitute v_p of (63) into the equation (64), we get a transcendental equation in v_0 that we solve numerically to obtain the exit point.

As a consequence, we have the next result that shows the existence and uniqueness of the relaxation oscillation.

Theorem 5. Let P be the fold point on the critical manifold \mathcal{M}_0^1 . Also, suppose that the positive equilibrium point is at the normally hyperbolic repelling critical submanifold under the parametric restriction,

$$u_1 < u_p$$

and let Γ denote a small neighborhood on a singular trajectory γ_0 formed by alternating slow and fast trajectories $\mathcal{O}(\varepsilon)$ -away from the fold point. Then, for $0 < \varepsilon \ll 1$ there exists a unique attracting limit cycle $\gamma_\varepsilon \subset \Gamma$ such that $\gamma_\varepsilon \rightarrow \gamma_0$ (in Hausdorff sense) as $\varepsilon \rightarrow 0$.

Proof. In order to study the dynamics of the system (61), we define two sections of the flow as

$$\begin{aligned} \Delta^{\text{in}} &= \{(u_+, v) : u_+ \ll u_p, v \in (v_p - \delta, v_p + \delta)\}, \\ \Delta^{\text{out}} &= \{(u_+, v) : u_+ \ll u_p, v \in (v_0 - \delta^2, v_0 + \delta^2)\}, \end{aligned}$$

where δ is a sufficiently small positive number; see Figure 16.

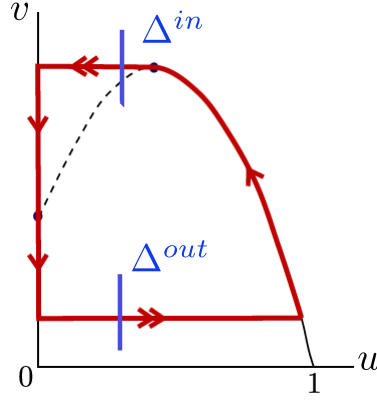


FIGURE 16. Sections of the flow: Δ^{in} and Δ^{out} .

We define a flow return map $\Pi : \Delta^{\text{in}} \rightarrow \Delta^{\text{in}}$, by the composition of the following two maps

$$\Phi : \Delta^{\text{in}} \rightarrow \Delta^{\text{out}}, \quad \Psi : \Delta^{\text{out}} \rightarrow \Delta^{\text{in}},$$

namely $\Pi = \Psi \circ \Phi$. For a fixed $0 < \varepsilon \ll 1$, the trajectory of system (61) starting at a point (u_+, v_+) on section Δ^{in} . From the analysis of the entry-exit function, we are able to say that this trajectory will be attracted to $\mathcal{M}_0^{0,a}$ and will leave $\mathcal{M}_0^{0,r}$ at point $(0, p(v_+))$, where p is the entry-exit function. Then, the trajectory jumps into the section Δ^{out} at the point $(u_+, p(v_+))$. Therefore, we can define the map Φ by entry-exit function as $\Phi(u_+, v_+) = (u_+, p(v_+))$.

On the other hand, for the map Ψ we consider two trajectories γ_ε^1 and γ_ε^2 starting from the section Δ^{out} . These trajectories get attracted toward $\mathcal{M}_\varepsilon^{1,a}$ where the slow flow is given by $\frac{du}{dt} = \frac{g(u, h(u, \varepsilon))}{h(u, \varepsilon)}$. Fenichel's theory and Theorem 2.1 of [21] guarantee that γ_ε^1 and γ_ε^2 contract exponentially toward each other even after jumping into the section Δ^{in} , so Π is, overall, a contraction. Finally, the contraction mapping theorem implies that the map Π has a unique fixed point, which gives rise to a unique relaxation oscillation cycle γ_ε that converges to the singular slow-fast cycle γ_0 as $\varepsilon \rightarrow 0$. \square

8. NUMERICAL ANALYSIS AND VALIDATION

In this section, MatCont is utilized as the principal instrument to examine the qualitative characteristics of the model and illustrate the analytical results through parameter variations.

For our simulations, we take the following setup of values of the parameters: $A = \frac{1}{2}$, $M = -\frac{1}{10}$, $\varepsilon = \frac{1}{20}$, while (C, Q) is going to be bifurcation parameters. In Figure 17, we present a codimension 2 bifurcation diagram showing the main organization of the important bifurcations. In particular, we can distinguish in Figure 17 regions where the positive equilibrium is unique and where it is not. We further notice that indeed, as shown in Appendix B, there is a Takens-Bogdanov bifurcation close to the point T_C . In there, we verify that the position of the Takens-Bogdanov point obtained numerically is indeed correct. In Figure 18, we show some representatives of the structure of the limit cycles in different regions of the parameter space. In particular, we verify the observation we made in ... that, as soon as multiple positive equilibria exist, the limit cycles, either stable or unstable, limit a homoclinic orbit.

9. CONCLUSIONS AND DISCUSSION

Within the context of predator-prey ecological dynamics, this paper focuses on the coexistence of predators and preys under the assumption that the prey exhibits fast dynamics. In addition to existing research in the context of slow-fast predator-prey systems such as [42], our main contribution is that we uncover new phenomena that involve the interaction between degenerate transcritical and Hopf singularities producing transitory canards and relaxation oscillations passing through those points.

It is important to recall that the study presented here focuses on the weak Allee effect, represented by $m < 0$ in system (1) (or $M < 0$ in system (2)), which guarantees the existence of the equilibrium point $T_C = (0, -MC)$, where if in addition $C = -AMQ$, then a degenerate transcritical singularity occurs. We have found that this point may behave in two ways depending on the parameters: on the one hand, it may behave like a stable node, and on the other hand, it may behave like a saddle. In the first case, orbits near T_C , which biologically speaking correspond to a low prey population and a predator population of $\approx -MC$, the system may evolve towards the extinction of the prey, or to a cycle of coexistence where the time spent near T_C is considerably large, and this is precisely due to the degenerate nature of the point.

Several research problem remain open. Here we discuss a few of them. First, we have found (see Sections 8 and B) the existence of a Takens-Bogdanov point. This naturally leads to interesting local dynamics and may influence the global ones. From Figure 17 this bifurcation occurs near the region where two positive coexisting equilibria are nearby, and so such a case may deserve extra attention. Another interesting problem, not discussed in this paper, is that of cyclicity [39, 40]. It would be interesting to consider it in the degenerate scenario.

APPENDIX A. EXPRESSION FOR THE TRACE OF THE JACOBIAN $\mathcal{J}(E_1)$

We derive an expression equivalent to $\frac{1}{Q} - J_{11}$, for this we will properly combine the equations (6)

$$\mathcal{U}_1^3 + (A - M - 1)\mathcal{U}_1^2 + \left(M - A - AM + \frac{1}{Q}\right)\mathcal{U}_1 + AM + \frac{C}{Q} = 0$$

and

$$\frac{1}{Q} - J_{11} = \frac{1}{Q} - \left(A - M + AM + 2(1 - A + M)\mathcal{U}_1 - 3\mathcal{U}_1^2\right),$$

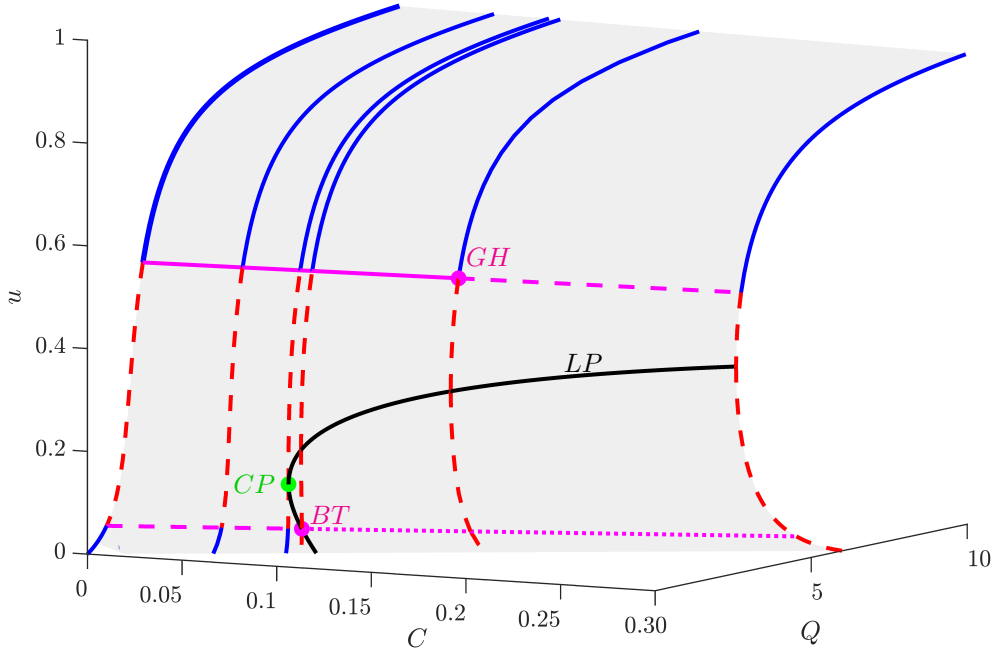


FIGURE 17. Equilibria of (16) and their bifurcations in a codimension 2 bifurcation diagram obtained via Matcont [7]. For this diagram we fix the parameters $A = \frac{1}{2}$, $M = -\frac{1}{10}$ and $\varepsilon = \frac{1}{50}$. The gray surface corresponds to equilibria. For fixed values of C , we show stable equilibria in blue and unstable equilibria in dashed red. These equilibria undergo a supercritical Hopf bifurcation along the solid magenta line and a subcritical one along the dashed magenta line. The dotted magenta line indicates neutral saddles. The black curve is a curve of limit points (LP), representing the region where the positive equilibrium is not unique. We further indicate a generalized Hopf point $GH = (u, v; C, Q) \approx (0.544, 0.306; 0.158, 2.292)$, a cusp point $CP = (u, v; C, Q) \approx (0.133, 0.128; 0.078, 1.657)$, and a Takens-Bogdanov point $BT = (u, v; C, Q) \approx (0.047, 0.076; 0.084, 1.721)$. See also Figure 18, which complements this diagram.

we obtain

$$\begin{aligned} \mathcal{U}_1 \left(\frac{1}{Q} - J_{11} \right) &= \left(\frac{1}{Q} - A + M - AM \right) \mathcal{U}_1 - (1 - A + M) \mathcal{U}_1^2 + \mathcal{U}_1^3 - (1 - A + M) \mathcal{U}_1^2 + 2\mathcal{U}_1^3 \\ &= -3 \left(AM + \frac{C}{Q} \right) - 2 \left(\frac{1}{Q} - A + M - AM \right) \mathcal{U}_1 + (1 - A + M) \mathcal{U}_1^2, \end{aligned}$$

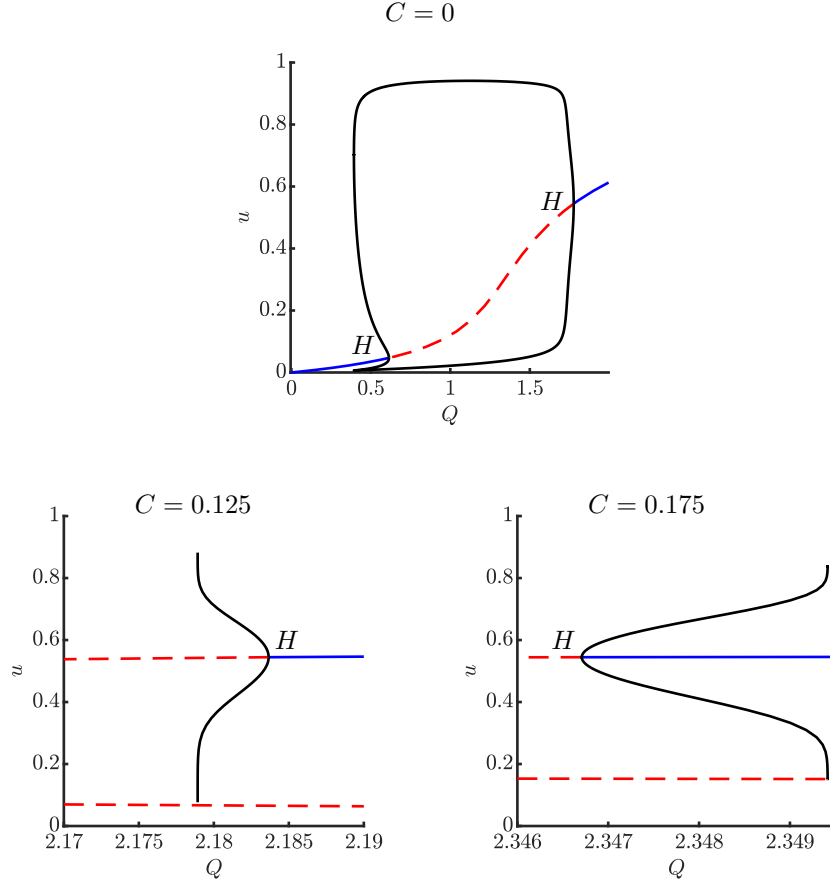


FIGURE 18. Bifurcation diagram highlighting the limit cycles (black curves) arising from Hopf bifurcations (compare with Figure 17). We show corresponding diagrams for $C = 0$, $C = 0.125$, and $C = 0.175$, the latter two around the GH point. Indeed, in the latter two cases, the limit cycles of the canard explosion are truncated and collide with the curve of equilibria, giving rise to a limit homoclinic orbit. This is also a numerical verification that the periodic orbits arising from a canard explosion end in a limit homoclinic orbit whenever the positive equilibrium is not unique, recall Remark 2.

solving for wJ_{11} we obtain

$$\mathcal{U}_1 J_{11} = 3 \left(AM + \frac{C}{Q} \right) + \mathcal{U}_1 \left((A - M - 1)\mathcal{U}_1 + 2 \left(\frac{1}{Q} - A + M - AM \right) + \frac{1}{Q} \right).$$

Thus, the trace and the determinant of \mathcal{J} are given by

$$\text{tr}(\mathcal{J}) = (\mathcal{U}_1 + C) \left((A - M + AM)\mathcal{U}_1 + 2(M + 1 - A)\mathcal{U}_1^2 - 3\mathcal{U}_1^3 - S(\mathcal{U}_1 + A) \right),$$

$$\det(\mathcal{J}) = S\mathcal{U}_1(\mathcal{U}_1 + A)(\mathcal{U}_1 + C)^2 \left(\frac{1}{Q} - (A - M + AM)\mathcal{U}_1 + 2(M + 1 - A)\mathcal{U}_1^2 - 3\mathcal{U}_1^3 \right).$$

APPENDIX B. ANALYTIC DETERMINATION OF THE TAKENS-BOGDANOV BIFURCATION

Motivated by the numerical findings of Section 8 we will show, in this appendix, that (2) exhibits a Takens-Bogdanov bifurcation of codimension 2, when E_1 approaches T_C . To achieve our aim, we shall first verify what are the parameter values for which both the trace and the determinant of the Jacobian matrix \mathcal{J} (8) evaluated at the point E_1 are equal to zero simultaneously.

Proposition 14. *The necessary and sufficient conditions for system (2) to have a Takens-Bogdanov bifurcation at $E_1 = (\mathcal{U}_1, \frac{\mathcal{U}_1 + C}{Q})$, that is such that $\text{tr } \mathcal{J}(E_1) = \det \mathcal{J}(E_1) = 0$, are*

$$\begin{aligned} A_* &= \frac{1}{2Q(\varepsilon + 3(\mathcal{U}_1 - 1)^2)} \left[\left(3C + Q(-3(\varepsilon + 2)\mathcal{U}_1 + \varepsilon - 6\mathcal{U}_1^3 + 14\mathcal{U}_1^2) + \mathcal{U}_1 + 3 \right)^2 \right. \\ &\quad \left. - 4Q(\varepsilon + 3(\mathcal{U}_1 - 1)^2)(C(3 - 6\mathcal{U}_1) + \mathcal{U}_1(Q\varepsilon(2\mathcal{U}_1 - 1) + Q(\mathcal{U}_1(3\mathcal{U}_1 - 10) + 5)\mathcal{U}_1 - 5\mathcal{U}_1 + 1)) \right]^{1/2} \\ &\quad + 3C - 3Q\varepsilon\mathcal{U}_1 + Q\varepsilon - 6Q\mathcal{U}_1^3 + 14Q\mathcal{U}_1^2 - 6Q\mathcal{U}_1 + \mathcal{U}_1 + 3, \end{aligned} \quad (65)$$

$$\begin{aligned} M_* &= \frac{1}{6Q(\mathcal{U}_1 - 1)^2} \left[\left(3C + Q(-3(\varepsilon + 2)\mathcal{U}_1 + \varepsilon - 6\mathcal{U}_1^3 + 14\mathcal{U}_1^2) + \mathcal{U}_1 + 3 \right)^2 \right. \\ &\quad \left. - 4Q(\varepsilon + 3(\mathcal{U}_1 - 1)^2)(C(3 - 6\mathcal{U}_1) + \mathcal{U}_1(Q\varepsilon(2\mathcal{U}_1 - 1) + Q(\mathcal{U}_1(3\mathcal{U}_1 - 10) + 5)\mathcal{U}_1 - 5\mathcal{U}_1 + 1)) \right]^{1/2} \\ &\quad - 3C - Q\varepsilon\mathcal{U}_1 + Q\varepsilon + 6Q\mathcal{U}_1^3 - 14Q\mathcal{U}_1^2 + 6Q\mathcal{U}_1 - \mathcal{U}_1 - 3. \end{aligned}$$

Proof. The Jacobian matrix corresponding to equations (2) evaluated in the point $E_1 = (\mathcal{U}_1, \frac{\mathcal{U}_1 + C}{Q})$ is

$$\mathcal{J}(E_1) = \begin{pmatrix} \mathcal{U}_1(\mathcal{U}_1 + C) \left((A - M + AM + 2(M + 1 - A)\mathcal{U}_1 - 3\mathcal{U}_1^2) \right) & -\mathcal{U}_1(\mathcal{U}_1 + C) \\ \frac{S(\mathcal{U}_1 + A)(\mathcal{U}_1 + C)}{Q} & -S(\mathcal{U}_1 + A)(\mathcal{U}_1 + C) \end{pmatrix}$$

We can find that $\text{tr } \mathcal{J}(E_1) = 0$ gives

$$M = \frac{AQ((\mathcal{U}_1 - 2)\mathcal{U}_1 - \varepsilon) + 3C + \mathcal{U}_1(-Q\varepsilon + Q\mathcal{U}_1 + 3)}{Q(A(2\mathcal{U}_1 - 3) + (\mathcal{U}_1 - 2)\mathcal{U}_1)}. \quad (66)$$

On the other hand, from $\det \mathcal{J}(E_1) = 0$ one computes the value of M , which is given by

$$M = \frac{AQ(2\mathcal{U}_1 - 1) + Q\mathcal{U}_1(3\mathcal{U}_1 - 2) + 1}{Q(A + 2\mathcal{U}_1 - 1)}. \quad (67)$$

Equating (66) and (67) and solving for A , we obtain the following expression:

$$\begin{aligned} A_* &= \frac{1}{2Q(\varepsilon + 3(\mathcal{U}_1 - 1)^2)} \left[\left(3C + Q(-3(\varepsilon + 2)\mathcal{U}_1 + S - 6\mathcal{U}_1^3 + 14\mathcal{U}_1^2) + \mathcal{U}_1 + 3 \right)^2 \right. \\ &\quad \left. - 4Q(\varepsilon + 3(\mathcal{U}_1 - 1)^2)(C(3 - 6\mathcal{U}_1) + \mathcal{U}_1(Q\varepsilon(2\mathcal{U}_1 - 1) + Q(\mathcal{U}_1(3\mathcal{U}_1 - 10) + 5)\mathcal{U}_1 - 5\mathcal{U}_1 + 1)) \right]^{1/2} \\ &\quad + 3C - 3Q\varepsilon\mathcal{U}_1 + Q\varepsilon - 6Q\mathcal{U}_1^3 + 14Q\mathcal{U}_1^2 - 6Q\mathcal{U}_1 + \mathcal{U}_1 + 3, \end{aligned}$$

Now, if we substitute this last value into (67), it follows that

$$M_* = \frac{1}{6Q(\mathcal{U}_1 - 1)^2} \left[\left(3C + Q(-3(\varepsilon + 2)\mathcal{U}_1 + \varepsilon - 6\mathcal{U}_1^3 + 14\mathcal{U}_1^2) + \mathcal{U}_1 + 3 \right)^2 \right. \\ \left. - 4Q(\varepsilon + 3(\mathcal{U}_1 - 1)^2)(C(3 - 6\mathcal{U}_1) + \mathcal{U}_1(Q\varepsilon(2\mathcal{U}_1 - 1) + Q(\mathcal{U}_1(3\mathcal{U}_1 - 10) + 5)\mathcal{U}_1 - 5\mathcal{U}_1 + 1)) \right]^{1/2} \\ - 3C - Q\varepsilon\mathcal{U}_1 + Q\varepsilon + 6Q\mathcal{U}_1^3 - 14Q\mathcal{U}_1^2 + 6Q\mathcal{U}_1 - \mathcal{U}_1 - 3.$$

□

To illustrate that Proposition 14 aligns with the numerical findings presented in Figure 17, we set the parameter values to those indicated in the caption of Figure 17, namely $C = 0.084$, $Q = 1.721$, $\varepsilon = S = 0.02$ and $\mathcal{U}_1 = 0.047$. This yields $A_* = 0.493075 \approx \frac{1}{2}$ and $M_* = -0.114541 \approx -\frac{1}{10}$. As a consequence, the numerical data and Proposition 14 are in agreement.

ACKNOWLEDGEMENTS

Roberto Albarrán García was supported by a PhD scholarship from CONACYT, México.

REFERENCES

- [1] C. Arancibia-Ibarra and J. Flores. Dynamics of a Leslie-Gower predator-prey model with Holling type II functional response, Allee effect and a generalist predator. *Math. Comput. Simul.*, 188(2):1–22, 2021.
- [2] G. Birkhoff and G.-C. Rota. *Ordinary differential equations*. John Wiley & Sons, Inc., New York, fourth edition, 1989.
- [3] F. Courchamp, L. Berec, and J. Gascoigne. *Allee effects in ecology and conservation*. Oxford University Press, Oxford, 2008.
- [4] P. De Maesschalck, T. S. Doan, and J. Wynen. Intrinsic determination of the criticality of a slow-fast Hopf bifurcation. *J. Dynam. Differential Equations*, 33(4):2253–2269, 2021.
- [5] P. De Maesschalck, F. Dumortier, and R. Roussarie. *Canard cycles—from birth to transition*, volume 73 of *Ergebnisse der Mathematik und ihrer Grenzgebiete. 3. Folge. A Series of Modern Surveys in Mathematics [Results in Mathematics and Related Areas. 3rd Series. A Series of Modern Surveys in Mathematics]*. Springer, Cham, [2021] ©2021.
- [6] P. De Maesschalck and S. Schechter. The entry-exit function and geometric singular perturbation theory. *J. Differential Equations*, 260(8):6697–6715, 2016.
- [7] A. Dhooge, W. Govaerts, and Y. A. Kuznetsov. Matcont: A matlab package for numerical bifurcation analysis of odes. *ACM Trans. Math. Softw.*, 29:141–164, 2003.
- [8] F. Dumortier. Techniques in the theory of local bifurcations: blow-up, normal forms, nilpotent bifurcations, singular perturbations. In *Bifurcations and periodic orbits of vector fields (Montreal, PQ, 1992)*, volume 408 of *NATO Adv. Sci. Inst. Ser. C: Math. Phys. Sci.*, pages 19–73. Kluwer Acad. Publ., Dordrecht, 1993.
- [9] F. Dumortier and R. Roussarie. Canard cycles and center manifolds. *Mem. Amer. Math. Soc.*, 121(577), 1996.
- [10] K. Fang, Z. Zhu, F. Chen, and Z. Li. Qualitative and bifurcation analysis in a Leslie-Gower model with Allee effect. *Qual. Theory Dyn. Syst.*, 21(3):Paper No. 86, 19, 2022.
- [11] N. Fenichel. Geometric singular perturbation theory for ordinary differential equations. *J. Differential Equations*, 31(1):53–98, 1979.
- [12] H. I. Freedman. *Deterministic mathematical models in population ecology*, volume 57 of *Monographs and Textbooks in Pure and Applied Mathematics*. Marcel Dekker, Inc., New York, 1980.
- [13] Y. Gao and S. Yao. Dynamical analysis of a modified Leslie-Gower Holling-type II predator-prey stochastic model in polluted environments with interspecific competition and impulsive toxicant input. *J. Biol. Dyn.*, 16(1):840–858, 2022.
- [14] E. Gonzalez-Olivares and A. Rojas-Palma. Global stability in a modified Leslie-Gower type predation model assuming mutual interference among generalist predators. *Math. Biosci. Eng.*, 17(6):7708–7731, 2020.
- [15] J. Guckenheimer and P. Holmes. *Nonlinear oscillations, dynamical systems, and bifurcations of vector fields*, volume 42 of *Applied Mathematical Sciences*. Springer-Verlag, New York, 1990.
- [16] G. Hek. Geometric singular perturbation theory in biological practice. *Journal of mathematical biology*, 60:347–86, 05 2009.

- [17] C. Holling. The components of predation as revealed by a study of small-mammal predation of the european sawfly. *Can. Entomol.*, 91:293–320, 1959.
- [18] C. Holling. Some characteristics of simple types of predation and parasitism. *Can. Entomol.*, 91:385–398, 1959.
- [19] H. Jardón-Kojakhmetov and C. Kuehn. A survey on the blow-up method for fast-slow systems. In *Mexican mathematicians in the world—trends and recent contributions*, volume 775 of *Contemp. Math.*, pages 115–160. Amer. Math. Soc., [Providence], RI, 2021.
- [20] Q. J. A. Khan, E. Balakrishnan, and G. C. Wake. Analysis of a predator-prey system with predator switching. *Bull. Math. Biol.*, 66(1):109–123, 2004.
- [21] M. Krupa and P. Szmolyan. Extending geometric singular perturbation theory to nonhyperbolic points—fold and canard points in two dimensions. *SIAM J. Math. Anal.*, 33(2):286–314, 2001.
- [22] M. Krupa and P. Szmolyan. Extending slow manifolds near transcritical and pitchfork singularities. *Nonlinearity*, 14(6):1473–1491, 2001.
- [23] M. Krupa and P. Szmolyan. Geometric analysis of the singularly perturbed planar fold. In *Multiple-time-scale dynamical systems (Minneapolis, MN, 1997)*, volume 122 of *IMA Vol. Math. Appl.*, pages 89–116. Springer, New York, 2001.
- [24] C. Kuehn. *Multiple time scale dynamics*, volume 191. Springer, 2015.
- [25] P. H. Leslie and J. C. Gower. The properties of a stochastic model for the predator-prey type of interaction between two species. *Biometrika*, 47:219–234, 1960.
- [26] J. Li, S. Li, and X. Wang. Canard, homoclinic loop, and relaxation oscillations in a Lotka-Volterra system with Allee effect in predator population. *Chaos*, 33(7):Paper No. 073130, 14, 2023.
- [27] A. J. Lotka. *Elements of Physical Biology*. Williams and Wilkins, Baltimore, 1925.
- [28] D. Ludwig, D. D. Jones, and C. S. Holling. *Qualitative analysis of insect outbreak systems: the spruce budworm and forest*, pages 547–564. University of Chicago Press, Chicago, 2022.
- [29] S. Muratori and S. Rinaldi. Remarks on competitive coexistence. *SIAM J. Appl. Math.*, 49(5):1462–1472, 1989.
- [30] J. Murray. *Mathematical biology*. Springer-Verlag, NY, 2nd edition edition, 2002.
- [31] H. Qiu and S. Guo. Bifurcation structures of a Leslie-Gower model with diffusion and advection. *Appl. Math. Lett.*, 135:Paper No. 108391, 6, 2023.
- [32] D. Sahoo and G. Samanta. Oscillatory and transient dynamics of a slow-fast predator-prey system with fear and its carry-over effect. *Nonlinear Anal. Real World Appl.*, 73:Paper No. 103888, 39, 2023.
- [33] S. J. Schreiber. Allee effects, extinctions, and chaotic transients in simple population models. *Theoretical Population Biology*, 64(2):201–209, 2003.
- [34] J. Shen. Canard limit cycles and global dynamics in a singularly perturbed predator-prey system with non-monotonic functional response. *Nonlinear Anal. Real World Appl.*, 31:146–165, 2016.
- [35] N. C. Stenseth, W. Falck, O. Bjornstad, and C. Krebs. Population regulation in snowshoe hare and canadian lynx: Asymmetric food web configurations between hare and lynx. *Proceedings of the National Academy of Sciences of the United States of America*, 94:5147–52, 06 1997.
- [36] F. Takens. Constrained equations; a study of implicit differential equations and their discontinuous solutions. In P. Hilton, editor, *Structural Stability, the Theory of Catastrophes, and Applications in the Sciences*, pages 143–234, Berlin, Heidelberg, 1976. Springer Berlin Heidelberg.
- [37] V. Volterra. Variazioni e fluttuazioni del numero d’individui in specie animali conviventi. *Mem. Acad. Lincei*, 6(2):31–113, 1926.
- [38] Z. Wen and T. Shi. Existence and Uniqueness of a Canard Cycle with Cyclicity at Most Two in a Singularly Perturbed Leslie–Gower Predator–Prey Model with Prey Harvesting. *Internat. J. Bifur. Chaos Appl. Sci. Engrg.*, 34(3):Paper No. 2450036, 2024.
- [39] J. Yao, J. Huang, and R. Huzak. Cyclicity of slow–fast cycles with two canard mechanisms. *Chaos*, 34(5):Paper No. 053112, 11, 2024.
- [40] J. Yao and R. Huzak. Cyclicity of the limit periodic sets for a singularly perturbed leslie–gower predator–prey model with prey harvesting. *Journal of Dynamics and Differential Equation*, 2022.
- [41] L. Zhong and J. Shen. Degenerate transcritical bifurcation point can be an attractor: A case study in a slow–fast modified leslie–gower model. *Qual. Theory Dyn. Syst.*, 21(76), 2022.
- [42] Z. Zhu and X. Liu. Canard cycles and relaxation oscillations in a singularly perturbed Leslie-Gower predator-prey model with Allee effect. *Internat. J. Bifur. Chaos Appl. Sci. Engrg.*, 32(5):Paper No. 2250071, 23, 2022.

DEPARTAMENTO DE MATEMÁTICAS, UAM–IZTAPALAPA, 09310 IZTAPALAPA, MEXICO CITY, MEXICO.

JOHANN BERNOULLI INSTITUTE FOR MATHEMATICS AND COMPUTER SCIENCE, UNIVERSITY OF GRONINGEN, P.O.
BOX 407, 9700 AK, GRONINGEN, THE NETHERLANDS

Email address: `albarrangr74@live.com.mx`, `mar@xanum.uam.mx`, `h.jardon.kojahmetov@rug.nl`